Crystal Engineering of Robust Metal-Organic Frameworks for Applications in Capture of Carbon Dioxide

ISHEKUDZWAI BLESSED GUDYANGA

(R153842B)

Submitted in fulfilment of the degree of Master of Philosophy in Chemistry in the Department of Chemical Sciences.

Midlands State University, Zimbabwe

Supervisor: Dr. G. Mehlana

September 2023

Declaration

I, Gudyanga Ishekudzwai Blessed (R153842B), hereby make this declaration that the thesis titled '**Crystal engineering of robust metal-organic frameworks for applications in capture of carbon dioxide**' is my own work, and has not been submitted to this or any other university for any degree requirements, or otherwise. In cases where secondary information or otherwise has been used in the thesis, it has duly been acknowledged and referenced.

Signature …….

Date ……..

Approval

This Masters dissertation titled “Crystal engineering of robust metal organic frameworks for applications in capture of carbon dioxide”, by Gudyanga Ishekudzwai. Blessed meets the regulations governing the award of Master of Philosophy in Chemistry, Midlands State University, Zimbabwe and is approved for its contribution to knowledge and literary presentation.

Supervisor …….

Date ……

Acknowledgements

I am eternally grateful to:

Dr Gift Mehlana, for his invaluable supervision and assistance throughout my master's studies.

Professor Ocean Cheung, Department of Materials Science and Engineering, Uppsala University, for assistance with gas sorption analyses.

Professor Lars Ohrstrom, Department of Chemistry and Chemical Engineering, Chalmers University of Technology, for support in collecting single crystal X-ray data.

Dr Hong Su, Department of Chemistry, University of Cape Town, for support in collecting single crystal X-ray data.

Midlands State University Department of Chemical Sciences did an excellent job. Thank you for all of your insightful inquiries, helpful recommendations, and excellent training during my studies.

For their moral support and late-night feedback sessions, I had the pleasure of working with Tatendaishe Blessing and Johannes Hungwe.

Lastly, I would be remiss if I did not mention my family, particularly my parents, Professor Ephias Gudyanga and Dr Anna Gudyanga, and the love of my life Lysa. Their faith in me has kept my attitude and motivation up throughout this journey.

Abstract

The atmospheric concentration of carbon dioxide gas (CO_2) is of global concern given its continued rise. Burning of fossil fuel has increased since the beginning of the industrial revolution, which then increased the atmospheric CO_2 concentration to > 400 ppm from 280 ppm. CO_2 has an effect of trapping the sun's heat, and is believed to be one of the cardinal contributors of global warming. In order to make improvements to the CO_2 problem, carbon capture techniques have been proposed. MOFs are porous structures constructed from the coordinative bonding between metal ions and organic linkers or bridging ligands. Thus, having an enormous choices of metal clusters and organic linkers, MOFs possess a wide range of surface area, pore volume and functionality, and this has contributed to the consideration of them being versatile materials for storage, separation, and catalysis, etc. Therefore, there is need to synthesise MOFs which capture CO_2 and convert it into useful chemicals such as methanol and formic acid for industrial application. Linker 2,2'-bipyridine-5,5'-dicarboxylic acid and ceric metal salt $Ce(NO_3)_3{\cdot}6H_2O$ were used in this study. Two MOFs were synthesised by solvothermal method. These were characterised by TGA, PXRD, FTIR, Potentiostat Galvanostat and Gas Sorption. The two MOFs **MSU-3** and **MSU-4** were thermally and chemically stable. The thermal and chemical stability observed in the MOFs emanated from the presence of the rod secondary building unit, which are linked by the pyridyl carboxylate linker to give three dimensional structures. CO_2 adsorption studies of the MOFs revealed a low uptake of the gas in comparison to those MOFs reported literature. **MSU-3a** and **MSU-4a** was tested for electroactivity. Also, resistivity was tested using electrical impedance spectroscopy. It was found out that both MOFs had a lower interfacial electron transfer resistance.

Acronyms

1D: One dimensional

2D: Two dimensional

3D: Three dimensional

Ce: Cerium

CCDC: Cambridge Crystallographic Data Centre

CO_2: Carbon dioxide

CSD: Cambridge Structural Database

CV: Cyclic Voltammetry

DEF: Diethylformamide

DMF: Dimethylformamide

EDS: Energy Dispersive X-ray Spectroscopy

EIS: Electrochemical Impedance Spectroscopy

Eu: Europium

FTIR: Fourier Transform Infrared

GCE: Glass Carbon Electrode

HKUST: Hong Kong University of Science and Technology

H_2bpdc: 2,2'-bipyridine-5,5' dicarboxylic acid

ILs: Ionic Liquids

IRMOF: Isoreticular metal organic framework

IUPAC: International Union of Pure and Applied Chemistry

LAG: Liquid Assisted Grinding

MOF: Metal-organic framework

NMR: Nuclear Magnetic Resonance

NDC: Napthalenedicarboxylic acid

PCPs: Porous Co-ordination Polymers

PSM: Post-synthetic modification

PXRD: Powder X-ray Diffraction

SBU: Secondary building unit

SCXRD: Single Crystal X-ray Diffraction

SEM: Scanning Electron Microscopy

TGA: Thermogravimetric Analysis

Yb: Ytterbium

Table of Contents

Chapter 1: Introduction

1.1 Introduction

The goal of this chapter is to present scenes for the crystal engineering project, and describe how metal-organic frameworks (MOFs) have developed in terms of design principles, synthesis, and significant factors affecting MOF structures.

1.2 Crystal engineering

The aim of crystal engineering is to construct supramolecular structures using rational synthetic methods that use the wide range of possible intermolecular interactions.[1] To create approaches for crystal synthesis, it is critical to comprehend the nature of the intermolecular interactions that bring the constituent molecules together into supramolecular arrays. New materials with intriguing properties have been created by building one-, two-, and three-dimensional (1-D, 2-D, and 3-D) metal-organic frameworks (MOFs) employing coordinate bonds.[2]

The reason why both zeolite and MOFs are microporous crystals with permanent porosity is because they can be produced by essentially identical solvothermal processes. It is also because several successful zeolite growth and morphology engineering attempts were made before MOF discovery.

The crystallisation studies on polycrystalline MOF films have been significantly influenced by the crystal engineering knowledge developed on zeolites.[3] As a result, the early breakthroughs in MOF films profited from the knowledge of how to make zeolite films under somewhat difficult synthesis circumstances. Despite this specific history, its crucial to understand the differences between MOFs and zeolites in terms of their structural chemistry, and synthesis method.

MOFs are made up of a weaker coordination bond between an organic linker and a metal node than zeolites, covalently bonded. The growth process and associated kinetics are also affected by this change in chemical structure. While there has not been a model for zeolite growth that is universally accepted, the model most frequently attributed is a non-classical growth mechanism in which growth occurs alongside the formation of an amorphous gel and involves a mixture of primary and secondary building units as well as precursor nanoparticles.

The *in-situ* growth and the seeded secondary growth are the two basic categories into which the synthesis pathways for a high-quality polycrystalline film can be divided. The *in-situ* method's greatest benefit is its enormous capacity for scaling. The procedure is straightforward, but getting a defect-free membrane this way can be difficult and frequently calls for a careful optimisation of the synthesis conditions.

It is crucial to direct the crystallisation process so that it occurs mostly on the porous support's surface rather than in solution. Popular methods to achieve this include (i) functionalising the surface of the support with an organic linker that has an affinity for the metal ions, (ii) using an interfacial method in which the metal ions and linker molecules are dissolved in separate solutions and react at the interface, and (iii) coating the surface of the substrate with a metal oxide layer to increase the interaction with the ligand.[4]

An ideal crystallisation chemistry for the synthesis of polycrystalline membranes should enable the synthesis of a defect-free membrane with independent control over grain size, membrane thickness, and orientation while obviating pinholes. This is because seeded secondary growth is a type of polycrystalline growth. A typical technique for producing a well-intergrown, thin, defect-free MOF membrane involves

seeding followed by secondary growth, which is an idea taken from zeolite membranes. When opposed to a direct growth procedure, this approach enables more control over particle size, membrane thickness, and orientation because the nucleation and growth processes are separated. The formation and attachment of a high density of tiny crystals (seeds) on a selected substrate are essential for the success of this approach.[3,5]

1.3 Metal-Organic Frameworks

MOFs are porous, crystalline materials made up of metal clusters linked by organic linkers.[6] Since 1972, there has been an increase in interest in these structures, with about 70 000 MOF entries in the Cambridge Structural Database (CSD), a collection of small molecule crystal structures, by 2016 (Figure 1.1).[7] MOFs, which have customisable pore diameters and huge surface areas, have piqued the curiosity of researchers for their prospective applications as storage materials in catalysis[8], separation chemistry[9], and luminescence.[10]

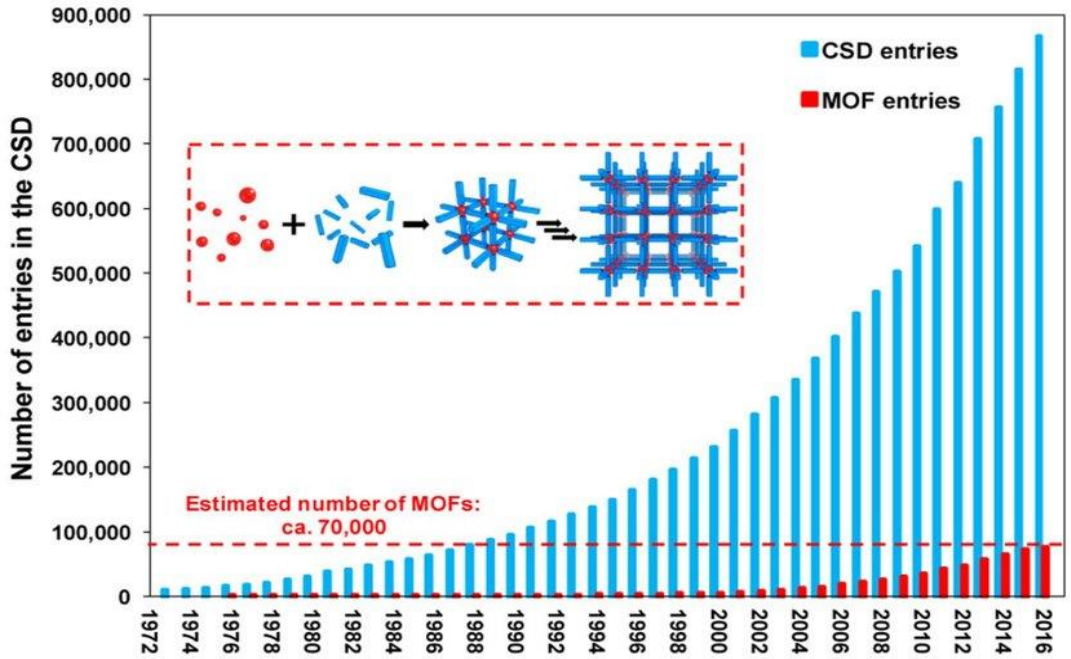

Figure 1.1: Graph depicting the development of CSD and MOF entries since 1972.[11]

Despite substantial study into the synthesis and characterisation of MOFs, classification remains a challenge. MOFs are sometimes referred to as coordination polymers in broader language, which has, understandably, caused some confusion in the literature due to nomenclature inconsistencies. A coordination polymer is a coordination molecule that contains repeated coordination units.[12] Coordination polymers, according to this concept, do not have to be crystalline in nature. A coordination network is defined as a coordination complex that extends in one dimension (with cross-links between two or more separate chains, for example) or extends in two or three dimensions.[13]

The early focus of research on 3D porous materials was on materials that had already been discovered in nature, such as zeolites, and exhibited a covalent structure that made such materials highly robust and valuable for applications such as ion exchange.[14] However, the presence of covalent bonds implies that these materials are extremely inflexible, and inserting weaker interactions such as coordination bonds, hydrogen bonds, or Π-Π interactions allows the framework structure to be flexible. Kitagawa et al. classified these two types of materials as second and third generation networks.[15] Among porous materials, coordination polymers made up of metal ‘nodes’ and organic linkers are particularly appealing because they offer limitless possibilities for rationally designing infinite networks that can respond dynamically and reversibly to environmental stimuli. All of these properties indicate that such materials are extremely adjustable and can be programmed to perform certain functions on command. MOFs are classified as a distinct class of materials due to their porosity and the implications that this property has for developing these materials for practical uses.[16]

Initially, most synthesis research concentrated on developing new MOFs that were more resistant to moisture, temperature variations, and other variables than MOF-5. One of the outcomes of such research was HKUST-1, a copper-based network with features that made it reasonable to consider how to synthesis these materials on a larger scale and in forms more suitable for industrial uses, such as pellets.[17]

Another goal of the researchers was to make the synthesis of large quantities of any MOF more efficient. This was both in terms of the number of reagents used, and the number of solvents involved. Not only as this for economic reasons, but it also due to the high environmental costs of using certain solvents in synthetic processes. Initially, most synthesis research concentrated on developing new MOFs that were more resistant to moisture, temperature variations, and other variables than MOF-5. One of the outcomes of such research was HKUST-1, a copper-based network with features that made it reasonable to consider how to synthesis these materials on a larger scale and in forms more suitable for industrial uses, such as pellets.[18]

MOFs are now primarily synthesised using five different processes, each of which has intrinsic advantages and downsides. This article describes materials synthesised using a typical solvothermal approach. Hence, the synthetic procedure will be detailed in further detail within this part, following a quick introduction to the alternatives open to researchers attempting to build MOFs.[19]

1.4 Synthesis of MOFs

The characteristics and functional elements of MOFs are directly influenced by the synthesis of metal-organic compounds, which also affects the crystallisation of the MOFs. By using different synthetic techniques, it is possible to modify the MOFs' architecture, pore structure, and size by selecting particular metal centres and organic

linkers.[11] Chemical functionalisation of linkers and post-modifications can alter the chemical characteristics of the resultant compounds.

1.4.1 Mechanochemical Synthesis

It is the most environmentally friendly way of synthesising MOFs because it uses little to no solvent and operates at very low temperatures. This approach is based on grinding the starting ingredients in a mortar-pestle or a ball-mill containing agate spheres, either without solvent or with a tiny amount of liquid (LAG, or liquid-assisted grinding). Mechanochemical synthesis is only appropriate for certain types of MOFs, a group that has recently been expanded with networks obtained via LAG by using the liquid as a structure directing factor or by inserting ions into the mixture to act as a templating agent for network formation. The fundamental constraint of this approach is the restricted number of substrates accessible.[20,21]

1.4.2 Sonochemical Synthesis

Sonochemical synthesis employs a horn-type Pyrex reactor fitted with a sonicator to create cavitation bubbles within the reaction medium, which means that when the bubbles collapse, the area around them heats incredibly quickly to 5000 K and then cools, resulting in the formation of very small crystallites at a much faster rate than other methods.[22,23]

1.4.3 Microwave-assisted Synthesis

The microwave-assisted synthesis is quite similar to traditional solvothermal synthesis in that it uses largely Teflon-lined jars containing the solvent and reagents, which are then placed in a microwave oven. The microwave system employs an oscillating

electric field to create rapid molecular mobility inside the medium, therefore rapidly heating the system. The capacity to control power within microwave equipment provides for a significant reduction in synthesis time at the expense of yield.[24,25]

1.4.4 Electrochemical Synthesis

The synthesis is carried out within an electrochemical cell which allows the metal ions required for network creation to diffuse into the solution from a metallic anode. To avoid metal deposition on the cathode, the reaction media is typically a protic solvent in which the organic linkers, and a conducting salt are dissolved. The advantages of such a method include the absence of a metal salt as a source of cations, and thus the absence of anions that could interfere with the reaction, the ability to run a continuous process and exceed quantities of product typically produced with batches of reagents, and the ability to tune various parameters such as solution conductivity or electrical current intensity in order to improve yield or tune characteristics such as morphology. This process is highly inefficient since the ohmic drop inside the solution necessitates a large energy investment to generate even modest product yields.[26,27,28]

1.4.5 Solvothermal Synthesis

While not the first method for obtaining MOFs, it is one of the simplest and commonly utilised. Several well-known networks, including MOF-5 and IRMOF-3, can be prepared by heating zinc salts in closed vessels to temperatures about 100 ^{o}C in solvents such as DEF (N,N-diethylformamide) or DMF (N,N-dimethylformamide). This method has been found to be exceptionally versatile due to the wide range of solvents that can be used, whether organic solvents or ionic liquids (ILs), as well as the wide range of experimental conditions that may be used.[29]

If less polydisperse distribution of crystallite size and smaller crystals overall is desired, stirring the mixture during the reaction should be considered while keeping in mind that the specific stirring rate has a major influence on the final product. Finally, the last significant component to consider is reaction time, which typically ranges from a few hours to a few days.[30]

Longer reaction times allow for the synthesis of less product, but can have a number of advantages such as an increase in product purity and a decrease in the number and quantity of other by-products produced in the reaction. This is because a kinetically favoured metastable phase may persist for a few hours, but an increase in reaction time to a few days is sometimes enough to only obtain the more thermodynamically stable product. Furthermore, giving the self-assembly process more time can boost the conversion rate from reagents to product, reducing the amount of unreacted material within the vessel.

When attempting to build crystals by solvothermal synthesis, there is additional variable, cooling rate, that is not directly related to other synthetic conditions, but can have a significant impact on parameters such as crystal size and by-product quantity. Cooling the solution quickly may preclude the development of crystals large enough to be employed in single crystal X-ray diffraction investigations, while cooling slowly may be impracticable in some cases.

There is a substantial number of variables that affect solvothermal synthesis while executing reactions, in a particular, solvent, assuming that the metal salt, organic linkers, and their mole ratios are kept consistent from experiment to experiment. The first and most obvious of these is the reagent concentration in solution, which can be adjusted to generate smaller crystallites, boost yield, and minimize the amount of

solvent required for each batch of reagents.[28] In most situations, however, the reaction is carried out in a dilute solution, which is optimal for producing larger crystals with size and quality acceptable for structure determination. Another critical variable is reaction temperature, which is heavily influenced by the vessel in which the reaction is carried out, as well as the heating mechanism, and most importantly, the solvent or mixture of solvents used in the reaction; most solvothermal methods typically require temperatures in the 90 ^{o}C to 150 ^{o}C range.[31]

1.5 Porosity

Porosity refers to the property of a material's host structure having 'holes' or channels that can be empty or inhabited by appropriately-sized molecules.[30] The property of porosity distinguishes MOFs from general coordination polymers, which have also been referred to as 'porous coordination polymers' or PCPs. Porosity is the foundation of numerous MOF applications, ranging from gas storage[32] and heterogeneous catalysis to drug delivery[30] and sensing.[33] PCP network crystal packing characteristics dictate whether voids or channels are created. Kitagawa et al. divided PCPs into three groups based on their 'kind' of porosity.[8] The porosity of the first kind, also known as the first generation or Type I, is critically dependent on the presence of guest molecules, i.e., the framework structure collapses if the guest is withdrawn. The framework structure is retained during guest removal in the second generation, or Type II, allowing for cyclic uptake/removal of guest molecules.

The frameworks of the third generation (Type III) are flexible and dynamic, responding to external stimuli-like as the presence of guest molecules, light, or electric fields. This enables for the reversible changes in channel widths and pore volume sizes. MOFs of the first and second generations are the most frequent, with only those of the second

and third generations acceptable for use. The most prevalent MOFs are first and second generation, with only those from the second and third generations appropriate for porosity applications. According to Barbour, a material's porosity may only be assigned if it can be demonstrated.[34]

As a result, the phrase ‘virtual porosity,’ was coined to refer to situations in which researchers simply remove atoms from a crystal structure and claim porosity based on the resulting voids. Barbour contends that this entails a prejudiced view on what can be described as ‘guest’ entities in the crystal structure without knowledge of whether these entities can diffuse throughout the crystal structure or what structural roles they play. The use of ‘porosity without pores’ refers to formations where no evident paths for the exit or admission of guest entities are obvious. Yet, it has been proved that molecules can exit and enter these materials. This demands significant dynamic alterations in the host framework to allow entities to migrate.

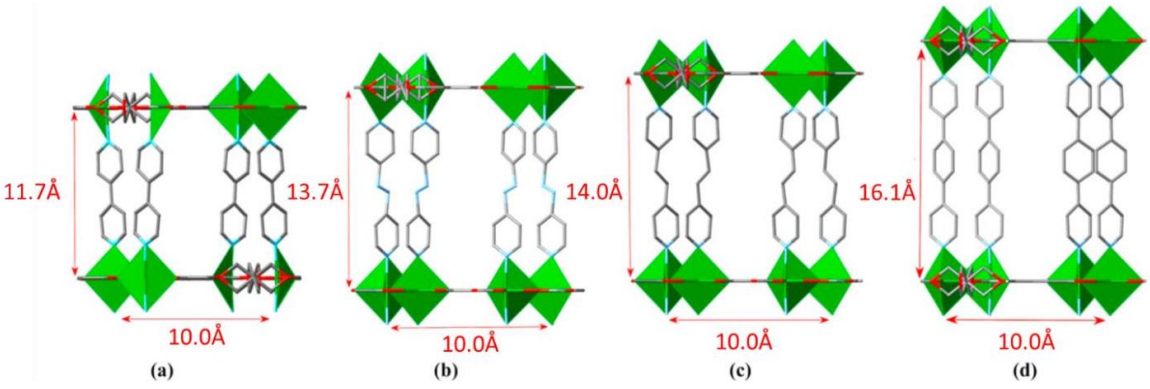

Figure 1.2: Schematic depiction of frameworks with several pillars: 4,4'-bipyridine (a), 4,4'-azopyrdine (b), 1,2-di(4-pyridyl)ethane (c), and 2-[4-(4-pyridinyl)phenyl] (d).pyridine.[35]

Controlling pore diameters in MOF porosity research is a crucial priority in order to 'tune' its usefulness in various applications. Controlling linker length is a viable technique to control pore size since it permits tuning of the pore size along a preferential route (if various ligands are employed in the same MOF) as shown in Figure. 1.2 or in all three directions (see Figure. 1.3). This possibility is well demonstrated by the IRMOF series (Fig 1.3), in which the same secondary building unit (SBU) is coupled by multiple ligands, resulting in MOFs with the same geometry but variable pore size dimensions.[36,37]

By increasing linker length, and thus pore size, it increases the possibility of interpenetration, which occurs when two or more entangled frameworks exist in the same crystal structure. Tiny pores or narrow channels between frameworks in interpenetrated structures may result in enhanced surface areas, which may be useful in sorption applications of tiny molecules such as hydrogen.[38]

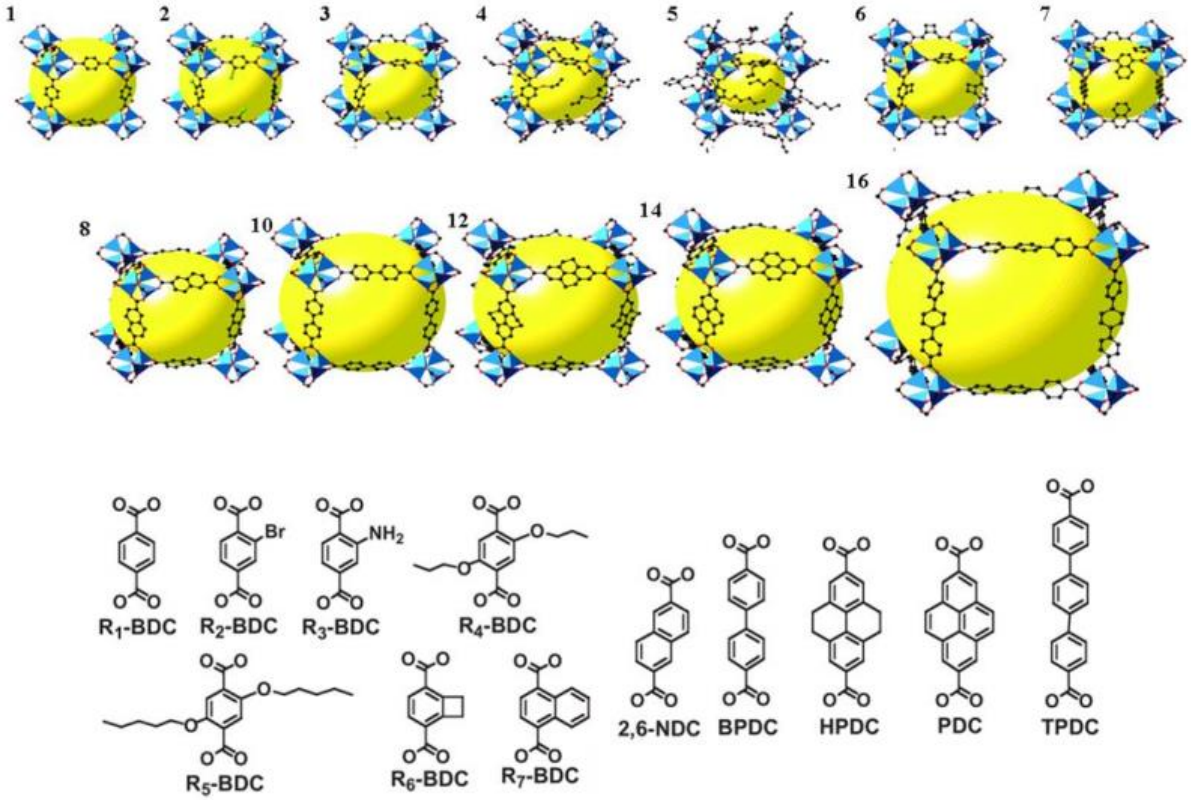

Figure 1.3: Labelled single crystal x-ray structures of IRMOF-n (n = 1 through 7, 8, 10, 12, 14, and 16). The following is the color scheme: Zn (blue polyhedron), O (red spheres), C (black spheres), Br (two green spheres), and amino-groups (three blue spheres). The strategy with the ligand that connects the SBUs is described below. R1 to R7 ligands are involved in the molecule from 1 to 7. The others are linked as follows: 2,6-NDC (Naphthalenedicarboxylic acid, 2,6-NDC)BPDC (Biphenyl-4,4′-dicarboxylic acid), -IRMOF-8 IRMOF-10, HPDC (4,5,9,10-tetrahydropyrene-2,7-dicarboxylic acid), IRMOF-12, PDC (pyrene-2,7-dicarboxylic acid), IRMOF-14, TPDC (p-Terphenyl-4,4″-dicarboxylic acid), IRMOF-16.[39]

1.6 Metal ions

Lanthanides, commonly known as rare earth elements, are a class of metallic elements with varying degrees of oxidation.[40] Most lanthanides, however, have a predominant oxidation state of +3 in their compounds due to the stability of their filled 4f electron shells because the 4f orbitals are insulated from the outer environment by the 5s and 5p orbitals, the 4f electrons participate in chemical bonding to a lesser extent.[41]

Lanthanides have the most stable and widespread oxidation state, which is +3.[42] Lanthanide ions lose three electrons in this state to achieve a stable configuration, which is generally written as $[Xe]4f^n$. The n value represents the number of electrons in the 4f orbital, which can range from 0 to 14 depending on the lanthanide element. Cerium (Ce), for example, has an oxidation state of +3 but can exist in the +4 oxidation state under specific conditions.[33]

It is crucial to remember that several lanthanides can have oxidation states other than +3. In addition to +3, europium (Eu) and ytterbium (Yb) can have oxidation states of +2 and +4. These alternate oxidation states, however, are rather rare and often require specialised chemical conditions or complexation with ligands to maintain.[43]

Overall, the +3 oxidation state for lanthanides is the most common and stable, reflecting the electrical arrangement of the 4f orbitals. However, under certain conditions, several lanthanides can exhibit different oxidation states, adding to the diversity and complexity of their chemical activity.

1.7 Linkers

In this project, a bipyridyl carboxylate linker, in particular, 2,2'-bipyridine-5,5' dicarboxylic acid (H_2bpdc) was employed for MOF synthesis. 2,2'-bipyridine 5,5' dicarboxylic acid is comprised of pyridyl and carboxylate moieties. In this study, the choice of the linker was made to facilitate MOF synthesis through the carboxylate moiety while bipyridyl units were exploited to anchor sites for catalytically active ruthenium metal. Carboxylate linkers are one of the most frequent types of linkers used in MOF synthesis due to their ability to make strong connections with the metal ions. The carboxylate groups have been shown to coordinate in a number of binding modes (eggs monodentate and bidentate) and have proven to stabilise the framework. Figure 1.4 depicts some of the various binding forms of H_2bpdc once fully deprotonated.[8]

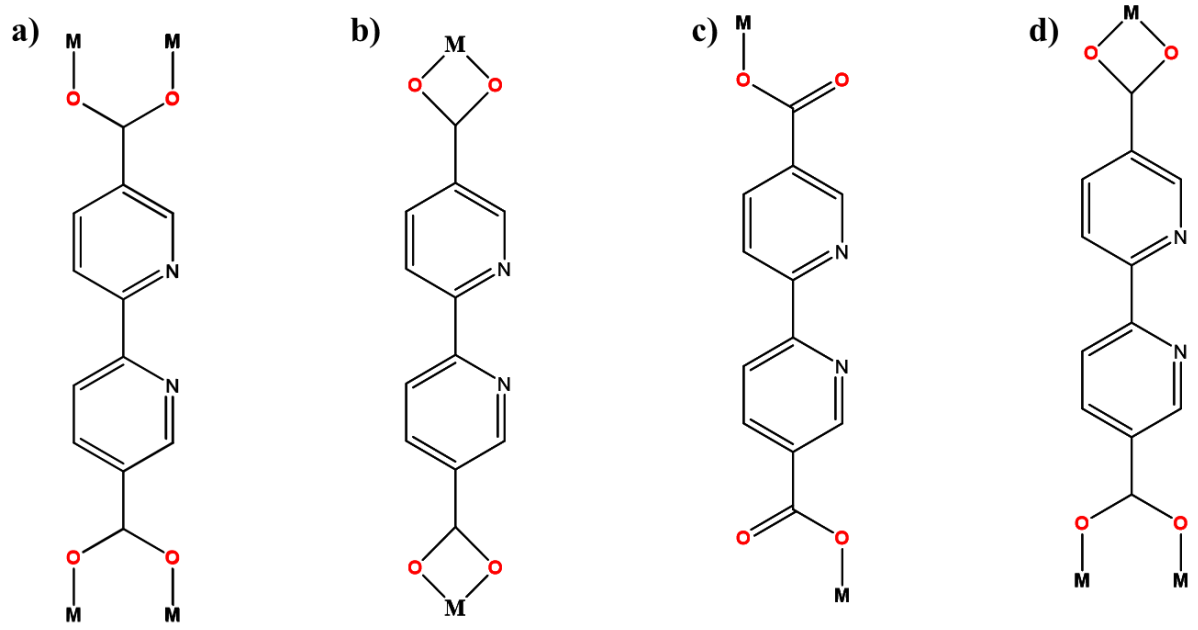

Figure 1.4: The coordination modes of the carboxylate. a) bridging bis-bidentate; b) chelating bis-bidentate; c) bis-monodentate and d) monodentate chelating and bridging manner.[8]

1.8 Gas Sorption

One of the key uses of MOFs is the capture and storage of carbon dioxide (CO_2) gas. As a greenhouse gas, CO_2 contributes to climate change, and its capture through industrial processes or straight from the atmosphere is vital for limiting its influence. MOFs offer an intriguing solution for CO_2 sorption due to their unique structural features. The enormous surface area of MOFs gives adequate space for CO_2 adsorption. The porosity of MOFs, commonly defined in terms of pore volume and specific surface area, allows for the physical trapping of CO_2 molecules within the framework. Furthermore, the porous structure of MOFs can be modified to enhance the interaction between CO_2 and the MOF surface, boosting the adsorption capacity.[30]

The interaction between CO_2 and MOFs happens through multiple methods, including physisorption and chemisorption. Physisorption refers to the non-covalent contact between CO_2 molecules and the MOF surface, typically caused by weak van der Waals forces.[32] Chemisorption includes the creation of chemical bonds between CO_2 and the MOF, resulting in more stable adsorption. The choice of MOF composition and functional groups on the organic linkers impacts the nature of the CO_2-MOF interaction.

To improve CO_2 sorption in MOFs, numerous techniques have been studied. One option is the synthesis of MOFs with large pore diameters and high surface areas to optimize gas uptake. Another technique involves functionalising the MOF surface with particular groups to boost the affinity for CO_2. For example, adding amine functional groups can promote the chemical interaction between CO_2 and the amine, leading to improved CO_2 capture.

The International Union of Pure and Applied Chemistry (IUPAC) has devised a classification system for adsorption isotherms, which categorizes the behaviour of adsorbates (molecules being adsorbed) on solid surfaces based on the shape of the isotherm curve as in Figure 1.5.[44] This classification system provides a standardised way to describe and compare adsorption processes. The IUPAC taxonomy of adsorption isotherms is as follows:

1.8.1 Type I: Langmuir-Isotherm

The Type I isotherm is characteristic of monolayer adsorption on a homogenous surface with a finite number of identical sites. The adsorption increases rapidly at low pressures but reaches a saturation point at higher pressures, indicating the creation of a monolayer. The isotherm is sigmoidal, with a fast rise followed by a plateau.

1.8.2 Type II: Non-Langmuirian Isotherm

The Type II isotherm suggests multilayer adsorption or adsorption on a surface with energetically heterogeneous locations. The adsorption rises continually with increasing pressure, without reaching a plateau. The isotherm is sigmoidal, similar to Type I, but without a well-defined saturation point.

1.8.3 Type III: Hysteresis Isotherm

The Type III isotherm is characterised by desorption not following the same path as adsorption, resulting in a loop in the isotherm curve. It often shows the existence of mesopores or macropores inside the adsorbent material, resulting to capillary condensation and desorption. The loop can be of many shapes, such as H1 (sharp), H2 (stepwise), or H3 (continuous).

1.8.4 Type IV: Cooperative Isotherm

The Type IV isotherm exhibits a sharp adsorption rise at low pressures, similar to Type I, but also shows a continuous increase in adsorption at higher pressures, similar to Type II. It shows the presence of both monolayer and multilayer adsorption, indicating cooperative adsorption activity. The isotherm is sigmoidal, with a blend of traits from Type I and Type II isotherms.

1.8.5 Type V: S-shaped or Discontinuous Isotherm

The Type V isotherm shows a slow increase in adsorption at low pressures, followed by a sudden increase, and ultimately reaching a plateau. It denotes the presence of a highly porous material with a complex pore structure, commonly related with hierarchical porous systems. The isotherm is sigmoidal, with a noticeable inflection point.

These IUPAC classes provide a systematic framework for characterising and comparing adsorption behaviour. It is crucial to remember that adsorption isotherms can also be modified by parameters such as temperature, pressure, surface area, and pore structure of the adsorbent material. Therefore, the IUPAC classification is a useful beginning point, but a comprehensive description of the adsorption process may require additional characterization and understanding of the specific system under inquiry.[45]

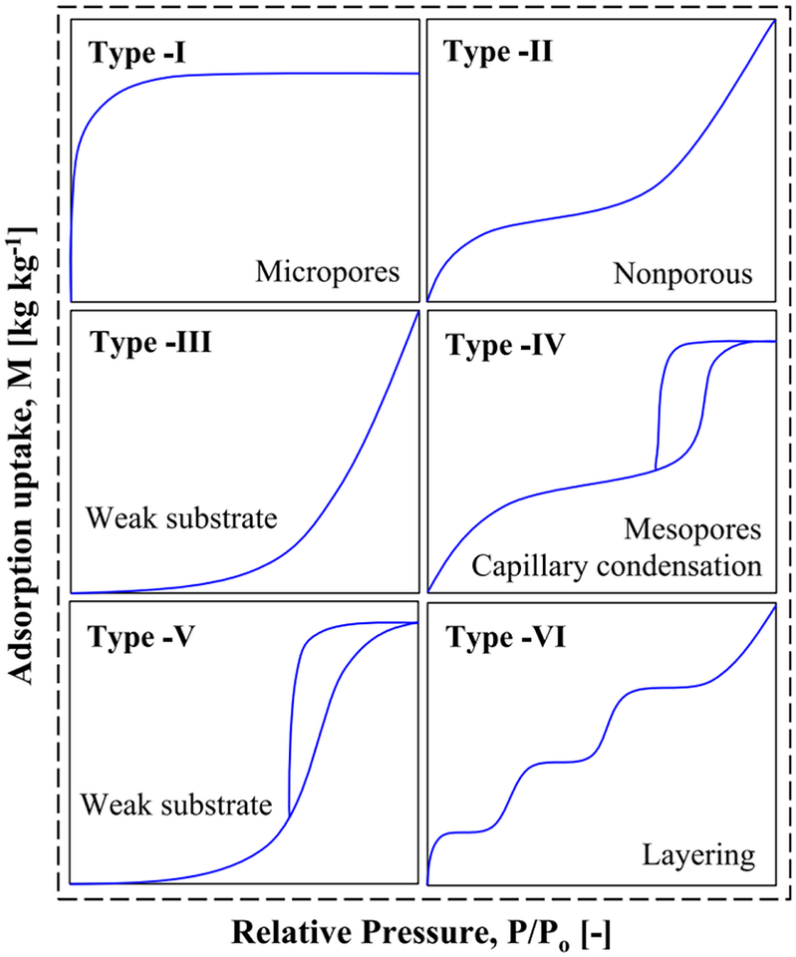

Figure 1.5: IUPAC classification of adsorption isotherms.[46]

1.9 Electrochemical Cells

Electrochemistry is the discipline of chemistry that explores the combination of chemical and electrical effects of a process. Electrolytic processes are reactions in which chemical changes occur on the passage of an electric current. The typical electrochemical cell consists of two electronic conductors which are also called electrodes and an ionic conductor, called the electrolyte. The charge transport in the electrodes occurs via the mobility of electrons whilst that in the electrolyte occurs via

the motion of both the positive and the negative ions.[47] Figure 1.6 depicts the configuration of a typical electrolysis cell.

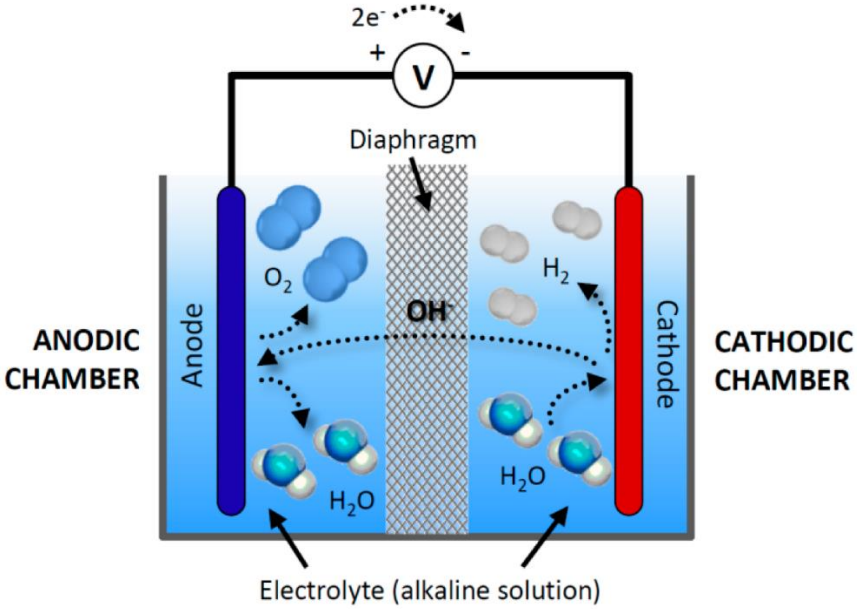

Figure 1.6: Typical electrolysis cell system. The anode and the cathode are immersed in the electrolyte and a voltage is applied to push the current from the anode to the cathode.[48]

Half-cell electrochemical reactions occur at each electrode, and the sum of the two individual half-cell reactions constitutes the cell's overall chemical reaction. In this experiment, the anode and cathode were made out of magnesium and steel electrodes respectively, while the electrolyte was urine. Urine conducts electricity. The chemical reactions at each electrode include: the oxidation of the magnesium anode, which allows the release of magnesium ions into the electrolyte; and the reduction of water to elemental hydrogen and hydroxide at the steel cathode.[49]

1.10 Electrochemical Cell Configurations

In a two-electrode set-up, the electrode at which the reaction of interest occurs is referred to as the working electrode, while the other is referred to as the counter electrode. In a three-electrode setup, a third electrode known as the reference electrode may also be employed. The reference electrode is an ideal non-polarisable electrode of known potential, such as Ag/AgCl in potassium chloride solution, and is usually placed close to the electrode on which the reaction of interest will occur to minimize the solution resistance between the two electrodes, which is sometimes referred to as the ohmic potential drop in the solution. The potential of the working electrode is determined using a reference. To do this, the potential of the reference must be constant, which can only be achieved if no current flows in the reference.[50]

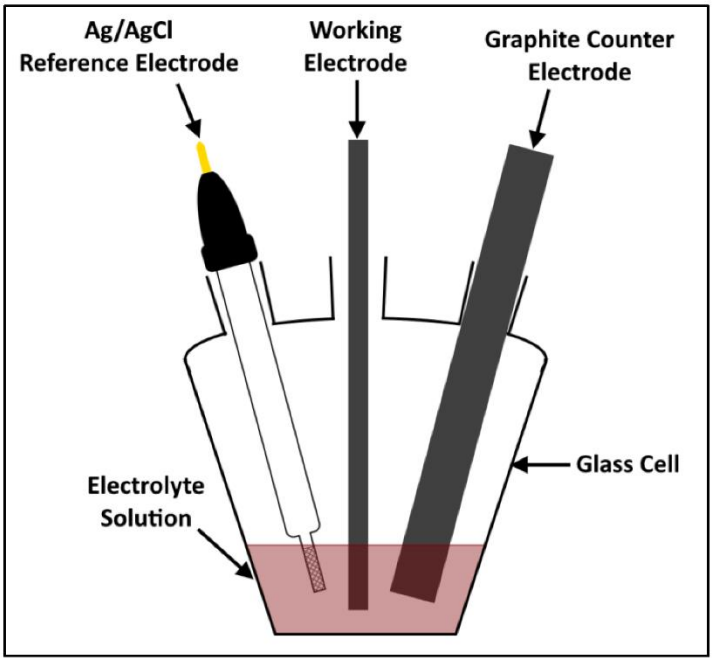

Figure 1.7: Three electrode system set-up.[51]

The potential difference between the working and reference electrodes may thus be precisely measured. Even though some uncompensated solution resistance persists, a reference electrode can be positioned extremely close to the working electrode using a fine capillary tip known as a Luggin-Haber capillary (Bard & Faulkner, 1980).

1.11 Motivation of the study

Due to their rich coordination geometry, excellent stability, capacity to build coordinated networks, and intriguing characteristics, MOFs based on lanthanides have attracted particular interest. The majority of lanthanide-based MOFs are water stable, and even more so than their equivalents based on transition metals. Given that lanthanide cations frequently contain a large number of coordinated solvent molecules, using them as building blocks for new MOFs can produce unsaturated metal sites that can be used for gas binding or Lewis acidic sites that can be used for catalysis.

1.12 Aim: To synthesize and characterize some Ceric MOFs using 2,2'-bipyride-5,5'-dicaboxylic acid and apply them for capturing of carbon dioxide.

1.13: Objectives

(i) Synthesise MOFs using 2,2'-bipyride-5,5'-dicaboxylic acid linker and Ce(III) metal salts.

(ii) Elucidate the structure of the synthesized MOFs using powder and single crystal X-ray diffraction.

(iii) Evaluate the thermal and chemical stability of the MOFs.

(iv) Modify glass carbon electrode (GCE) using MOFs and characterise using cyclic voltammetry (CV) and electrochemical impedance spectroscopy (EIS).

(v) demonstrate the efficacy of the MOFs in carbon dioxide capture.

1.14 References

1. Babu, D. J., He, G., Villalobos, L. F. & Agrawal, K. V. Crystal Engineering of Metal-Organic Framework Thin Films for Gas Separations. *ACS Sustain. Chem. Eng.***7**, 49–69 (2019).

2. Maarten Gérard Goesten, S. I. Crystal Engineering with Metal-Organic Frameworks. *Chem. Int.* **4**, 127 (2015).

3. Shunzhi Wang, Sarah S. Park, Cassandra T. Buru, Haixin Lin, Peng-Cheng Chen, Eric W. Roth, Omar K. Farha & Chad A. Mirkin. Colloidal crystal engineering with metal–organic framework nanoparticles and DNA. *Nat. Commun.***11**, 1–8 (2020).

4. Yap, M. H., Fow, K. L. & Chen, G. Z. Synthesis and applications of MOF-derived porous nanostructures. *Green Energy Environ.***2**, 218–245 (2017).

5. Vodyashkin, A. A., Sergorodceva, A. V., Kezimana, P. & Stanishevskiy, Y. M. Metal-Organic Framework (MOF)—A Universal Material for Biomedicine. *Int. J. Mol. Sci.***24**, 66−78 (2023).

6. Yingbo Zhao, Christopher S. Kley, Chenhui Zhu, Dohyung Kim, Song Lin, Christopher J. Chang, Omar M. Yaghi&Peidong Yang. Metal-Organic Frameworks for Electrocatalytic Reduction of Carbon Dioxide. *J. Am. Chem. Soc.***137**, 14129–14135 (2015).

7. Linfeng Liang, Caiping Liu, Feilong Jiang, Qihui Chen, Linjie Zhang, Hui Xue, Hai-Long Jiang, Jinjie Qian, Daqiang Yuan & Maochun Hong. Carbon dioxide capture and conversion by an acid-base resistant metal-organic framework. *Nat.*

*Commun.***8**, 453−460 (2017).

8. Botao Liu, Kowsalya Vellingiri, Sang-Hee Jo, Pawan Kumar, Yong Sik Ok & Ki-Hyun Kim. Recent advances in controlled modification of the size and morphology of metal-organic frameworks. *Nano Res.***11**, 4441–4467 (2018).

9. Sridhar, S., Smitha, B. & Aminabhavi, T. M. Separation of carbon dioxide from natural gas mixtures through polymeric membranes - A review. *Sep. Purif. Rev.***36**, 113–174 (2007).

10. Meili Ding, Robinson W. Flaig, Hai-Long Jiang & Omar M. Yaghi. Carbon capture and conversion using metal–organic frameworks and MOF-based materials. *Coord. Chem. Rev.***48**, 79–120 (2019).

11. Das, S., Kim, H. & Kim, K. Metal-Organic Frameworks History. *Inorg. Chem.***21**, 1–29 (2021).

12. Liang, J., Huang, Y. & Cao, R. Metal – organic frameworks and porous organic polymers for sustainable fixation of carbon dioxide into cyclic carbonates. *Coord. Chem. Rev.***33**, 412−420 (2017).

13. Cui, W. G., Zhang, G. Y., Hu, T. L. & Bu, X. H. Metal-organic framework-based heterogeneous catalysts for the conversion of C1 chemistry: CO, CO 2 and CH 4. *Coord. Chem. Rev.***387**, 79–120 (2019).

14. Yang Ming, Justin Purewal, Jun Yang, Chunchuan Xu, Mike Veenstra, Manuela Gaab, Ulrich Müller, Donald J. Siegel. Stability of MOF-5 in a hydrogen gas environment containing fueling station impurities. *Int. J. Hydrogen Energy* **41**, 9374–9382 (2016).

15. Kitagawa, S., Kitaura, R. & Noro, S. I. Functional porous coordination polymers.

*Angew. Chemie - Int. Ed.***43**, 2334–2375 (2004).

16. Tella, A. C., Olawale, M. D., Neuburger, M. & Obaleye, J. A. Synthesis and crystal structure of Cd-based metal-organic framework for removal of methyl-orange from aqueous solution. *J. Solid State Chem.***255**, 157–166 (2017).

17. Chongxiong Duan,Hang Zhang,Feier Li,Jing Xiao, Shaojuan Luo&Hongxia Xi. Hierarchically porous metal-organic frameworks: Rapid synthesis and enhanced gas storage. *Soft Matter* **14**, 9589–9598 (2018).

18. Pichon, A. & James, S. L. An array-based study of reactivity under solvent-free mechanochemical conditions - Insights and trends. *CrystEngComm* **10**, 1839–1847 (2008).

19. Links, D. A. Syntheses , structures and properties of silver – organic frameworks constructed.*Soft Matter* **4**, 10071–10081 (2011).

20. Pichon, A., Lazuen-Garay, A. & James, S. L. Solvent-free synthesis of a microporous metal-organic framework. *CrystEngComm* **8**, 211–214 (2006).

21. Li, B. & Ge, H. Highly selective electrochemical hydrogenation of alkynes: Rapid construction of mechanochromic materials. *Sci. Adv.***5**, 1–8 (2019).

22. Barua, S., Chattopadhyay, P., Phukan, M. M., Konwar, B. K. & Karak, N. Hyperbranched epoxy/MWCNT-CuO-nystatin nanocomposite as a high performance, biocompatible, antimicrobial material. *Mater. Res. Express***1**, (2014).

23. Zhanfeng Li, Jun Dong,Huixin Zhang,Yongqiang Zhang,Huiqi Wang,Xuejun Cui&Zonghua Wang. Sonochemical catalysis as a unique strategy for the fabrication of nano-/micro-structured inorganics. *Nanoscale Adv.***3**, 41–72

(2021).

24. Aniruddha, R., Sreedhar, I. & Reddy, B. M. MOFs in carbon capture-past, present and future. *J. CO_2 Util.***42**, 101297 (2020).

25. Linh Ho Thuy Nguyen, Hue Thi Thu Nguyen, Bao Quang Gia Le, Minh-Huy Dinh Dang, Trang Thi Thu Nguyen, Ngoc Xuan Dat Mai& Tan Le Hoang Doan. Microwave-assisted solvothermal synthesis of defective zirconium-organic framework as a recyclable nano-adsorbent with superior adsorption capacity for efficient removal of toxic organic dyes. *Colloids Interface Sci. Commun.***46**, 111-311 (2022).

26. Al-Saydeh, S. A. & Zaidi, S. J. Carbon Dioxide Conversion to Methanol: Opportunities and Fundamental Challenges. *Carbon Dioxide Chem. Capture Oil Recover.***56**, 3655−3699 (2018).

27. Yan-Ling Qiu, He-Xiang Zhong, Tao-Tao Zhang, Wen-Bin Xu, Pan-Pan Su, Xian-Feng&Hua-Min Zhang. Selective Electrochemical Reduction of Carbon Dioxide Using Cu Based Metal Organic Framework for CO2 Capture. *ACS Appl. Mater. Interfaces***10**, 2480–2489 (2018).

28. Al-Omari, A. A., Yamani, Z. H. & Nguyen, H. L. Electrocatalytic CO2 reduction: From homogeneous catalysts to heterogeneous-based reticular chemistry. *Molecules***23**, 1–12 (2018).

29. Upadhyay, P. & Srivastava, V. Carbon Sequestration: Hydrogenation of CO2 to Formic Acid. *Present Environ. Sustain. Dev.***10**, 13–34 (2016).

30. Remya, V. R. & Kurian, M. Synthesis and catalytic applications of metal–organic frameworks: a review on recent literature. *Int. Nano Lett.* **9**, 17–29 (2019).

31. Rumayor, M., Dominguez-Ramos, A. & Irabien, A. Formic Acid manufacture: Carbon dioxide utilization alternatives. *Appl. Sci.***8**, 1–12 (2018).

32. Kazemi, S. & Safarifard, V. Carbon dioxide capture in MOFs: The effect of ligand functionalization. *Polyhedron* **154**, 236–251 (2018).

33. Raghavan, K. Metal Organic Frameworks–Synthesis and Applications. Industrial Catalysis and Separations. *Int. Nano Lett.* **3**, 33−40 (2014).

34. Barbour, L. J. X-seed - A software tool for supramolecular crystallography. *J. Supramol. Chem.***1**, 189–191 (2001).

35. Du, M., Li, C. P., Liu, C. Sen & Fang, S. M. Design and construction of coordination polymers with mixed-ligand synthetic strategy. *Coord. Chem. Rev.***257**, 1282–1305 (2013).

36. Wang, Z., Tanabe, K. K. & Cohen, S. M. Accessing postsynthetic modification in a series of metal-organic frameworks and the influence of framework topology on reactivity. *Inorg. Chem.***48**, 296–306 (2009).

37. Perry, J. J., Perman, J. A. & Zaworotko, M. J. Design and synthesis of metal–organic frameworks using metal–organic polyhedra as supermolecular building blocks. *Chem. Soc. Rev.***38**, 1400–1417 (2009).

38. Waiapu Timothy McMillan, O. Characteristics and mechanisms of atrazine sorption to biochar for land remediation.*Int. Nano Lett.* **43**, 114−120 (2018).

39. Mohamed Eddaoudi, Jaheon Kim, Nathaniel Rosi, David Vodak, Joseph Wachter, Michael O'Keeffe& Omar M Yaghi. Systematic design of pore size and functionality in isoreticular MOFs and their application in methane storage. *Science (80).***295**, 469–472 (2002).

40. David Harvey. Theory and Instrumentation of GC Introduction. *Chromacademy* **2**, 17–18 (2019).

41. He, T., Zhang, L., Kour, G. & Du, A. Electrochemical reduction of carbon dioxide on precise number of Fe atoms anchored graphdiyne. *J. CO2 Util.***37**, 272–277 (2020).

42. Wang, Y. & Wöll, C. Chemical Reactions at Isolated Single-Sites Inside Metal–Organic Frameworks. *Catal. Letters* **148**, 2201–2222 (2018).

43. Linden, A. Chemistry and structure in Acta Crystallographica Section C. *Acta Crystallogr. Sect. C Struct. Chem.* **71**, 1–2 (2015).

44. Rowsell, J. L. C. & Yaghi, O. M. Metal-organic frameworks: A new class of porous materials. *Microporous Mesoporous Mater.***73**, 3–14 (2004).

45. Motkuri, R. K, Samanidou, V. F, Deliyanni, E. A. Metal organic frameworks–synthesis and applications. *Ind. Catal. Sep. Innov. Process Intensif.***1**, 61–104 (2014).

46. Wells, B. A. & Chaffee, A. L. Modeling gas separation in metal-organic frameworks. *Adsorption* **17**, 255–264 (2011).

47. Solmaz, R. & Kardaş, G. Electrochemical deposition and characterization of NiFe coatings as electrocatalytic materials for alkaline water electrolysis. *Electrochim. Acta* **54**, 3726–3734 (2009).

48. Iwasita, T. Electrocatalysis of methanol oxidation. *Electrochim. Acta* **47**, 3663–3674 (2002).

49. Junyu Liu, Luwei Peng, Yue Zhou, Li, Jing Fu, Jia Lin, Daniel Guay& Jinli Qiao. Metal-Organic-Frameworks-Derived Cu/Cu_2O Catalyst with Ultrahigh Current

Density for Continuous-Flow CO_2 Electroreduction. *ACS Sustain. Chem. Eng.* **7**, 15739–15746 (2019).

50. Shao, P., Yi, L., Chen, S., Zhou, T. & Zhang, J. Metal-organic frameworks for electrochemical reduction of carbon dioxide: The role of metal centers. *J. Energy Chem.* **40**, 156–170 (2020).

51. Senthil Kumar, R., Senthil Kumar, S. & Anbu Kulandainathan, M. Highly selective electrochemical reduction of carbon dioxide using Cu based metal organic framework as an electrocatalyst. *Electrochem. commun.* **25**, 70–73 (2012).

Chapter 2: Experimental

2.1 Introduction

This chapter describes the common synthetic procedures used to prepare MOFs. Also provided are several methods and tools for structural clarification and thorough characterisation.

2.2 Starting Materials

The organic linker 2,2'-bipyridine-5,5'-dicarboxylic acid (98% purity) and ceric metal salt $Ce(NO_3)_3 \cdot 6H_2O$ were purchased from Sigma-Aldrich, and used as received. Potassium Ferricyanide ($K_3[Fe(CN)_6]$) and Potassium Ferrocyanide ($K_4[Fe(CN)_6]$) were also purchased from Sigma Aldrich. Potassium Chloride (KCl) and Potassium Bromide (KBr) were obtained from Skylabs. The solvents N,N dimethyl formamide (99.8 % purity) and methanol (99.8 % purity) were purchased from Sigma-Aldrich and used as received unless otherwise mentioned.

2.3 General Synthesis of MOFs

With the aid of solvothermal synthesis approach, single crystals of MOFs were produced. The ligand and the metal salts were separately dissolved in DMF before being combined in the synthesis. Crystals were produced by heating the solution in the vials in an oven at a specific temperature. In the pertinent chapters, specific synthetic processes for the various metal organic frameworks will be covered.

2.4 X-Ray Diffraction

2.4.1 Single Crystal X-Ray Diffraction (SCXRD)

Single crystal X-ray diffraction is a technique which gives information on the molecular structure of the sample.[1] Information collected includes; crystal symmetry,[2] space groups,[3] unit cell dimensions,[4] volume and crystal size.[5] To determine whether the structure is new or known in the literature, unit cell parameters can be compared with online databases.

Under a microscope, good single crystals of the right size were chosen from the mother liquor and coated in paratone N oil to prevent solvent molecule loss or decomposition. The single crystals was trimmed to the desired size in cases where they were to be used. Structure determination for the MOFs were performed using a Bruker KAPPA APEX II DUO diffractometer equipped with a graphite monochoromated Mo-Kα radiation. (λ =0.71073 Å).

Data collections was performed at low temperatures of 173.11 K. Low temperatures ensured that solvent molecules remained in the crystal throughout the experiment. Unit cell refinement were performed using SAINT program.[6] Data was corrected for Lorentz-polarisation and absorption effects using the multi-scan method (SADABS.[7] The program XPREP[7] was used to confirm the space group of the structures. The structure solutions were achieved by direct methods (program SHELXS)[8] and refined anisotropically by full-matrix least-squares on F^2 using SHELXL[9] within the X-SEED[10] interface. The non-hydrogen atoms were located in the difference electron density maps and were refined anisotropically while all the hydrogen atoms were placed with geometric constraints and refined with isotropic temperature factors. For disordered

solvent molecules, the program SQUEEZE[11] was used to estimate the number of DMF molecules per asymmetric unit.

2.4.2 Powder X-Ray Diffraction (PXRD)

Powder X-ray diffraction (PXRD) is a rapid analytical technique primarily used for phase identification of a crystalline material and can provide information on unit cell dimensions.[12] Measurements for **MSU-3** and **MSU-4** were performed on a Bruker D2 Phaser 2nd Gen diffractometer[13] using Cu Kα-radiation at 298 K. X-rays were generated with a current flow of 10 mA and voltage of 30 kV. Crystals were removed from the mother liquor and dried on a filter paper before being analysed. The samples were then placed onto a zero-background sample holder and scanned over 2θ range 5 to 60° with a step of 0.35° increments. The experimental PXRD patterns recorded were plotted using Excel. The fully refined single-crystal structure coordinates were input into Mercury program to produce an idealised calculated PXRD pattern of the structure. The calculated pattern was compared with the experimental PXRD pattern to determine whether the integrity of the MOF was maintained.

2.5 Electrochemistry

2.5.1 Electrochemical Characterization

Electrochemical characterisation of electrode modifiers involves the study of the electrochemical behaviour of the modified electrodes which helps to evaluate electron transfer kinetics. Evaluation of electron transfer kinetics was investigated on modified electrodes using cyclic voltammetry and electrochemical impedance spectroscopy. Prior to use, the bare GCE was thoroughly polished on a pad with distilled water and then washed with distilled water between each polishing step. To remove any impurities, the GCE was sonicated for 5 min in distilled water and allowed to dry before

modification. The GCE was then modified using the drop-dry method, where 5 µL of the modifier (1mg/ml in DMF) was placed on the surface of the electrode and allowed to dry in an oven at 60°C. The electrodes were designated as MSU-3a/GCE and MSU-4a/GCE.

2.5.2 Cyclic voltammetry in 1mM $[Fe(CN)_6]^{3-/4-}$ solution.

Cyclic voltammetry was used for the investigation of electron transfer behaviour for the bare GCE, MSU-3a/GCE and MSU-4a/GCE in 1 mM $[Fe(CN)_6]^{3-/4-}$ in 0.1 M KCl at a scan rate of 100 mV/s from -0.2 to 0.6 V.

2.5.3 Scan rate studies in 1 mM $[Fe(CN)_6]^{3-/4-}$ solution.

Scan rate studies were performed in 1mM $[Fe(CN)_6]^{3-/4-}$ solution by using MSU-3a and MSU-4a electrode in order to determine the reaction kinetics of the modified electrode. The studies were carried out using cyclic voltammetry from -0.2 to 0.6 V at scan rates of 0.03 – 0.35 V/s.

2.5.4 Electrochemical impedance spectroscopy

Electrical impedance spectroscopy and Bode plots studies were investigated in 1 mM $[Fe(CN)_6]^{3-/4-}$ on the GCE to evaluate electron transfer resistance and structural difference of the modified electrodes, MSU-3a/GCE and MSU-4a/GCE.

2.6 Spectroscopic Analysis

2.6.1 Fourier Transform Infrared Spectroscopy (FTIR)

Infrared spectrum is an important record which gives sufficient information about the functional groups of a compound. Fourier Transform Infrared Spectra (FTIR) analysis of the samples was recorded in the range 400 to 4000 cm^{-1} on Nicolet 6700 Thermo-Scientific Fourier Transform Infrared spectrophotometer. The sample was mixed finely

with Potassium Bromide (KBr) in the ratio 1:100 respectively and were mounted on the spectrophotometer for data collection. The technique was used to establish the presence of distinct functional groups and the binding mode of the carboxylate moiety.

2.7 Thermogravimetric Analysis

Thermogravimetric analysis was utilized to predict the number of solvent molecules per asymmetric unit by quantifying the mass loss as a function of temperature. In relation to the stability of the framework, it was also used to calculate the decomposition temperature. Samples were surface dried on filter paper before analysis. TGA experiments were performed by weighing 2 and 5 mg samples onto an aluminum pan using a TA Discovery Instrument TA-Q50 with a heating rate of 10 °C min^{-1} at the range of 25–600 °C under a dry nitrogen purge gas flow of 50 $mLmin^{-1}$.

2.8 Chemical Stability Tests

The activated MOFs samples were soaked different solvents which include Methanol, Ethanol, Triethylamine, Tetrahydrofuran and water for 24 hours. These solvents are normally used for CO_2 hydrogenation. The solids recovered by filtration were washed thoroughly before recording FTIR spectra and PXRD patterns.

2.9 Gas Sorption Studies

Porosity and surface properties of **MSU-3** were analyzed by CO_2 sorption at 293 K in a Micromeritics ASAP 2020 (Norcross, GA) volumetric gas adsorption analyser. Isotherms of the MOF were also recorded using the same instrument at 293 K, and a water bath was used for temperature control. Prior to the adsorption measurements, the samples were degassed at 423 K for 12 h under dynamic vacuum (1 × 10–4 Pa) using a Micromeritic Smart VacPrep060 (Norcross, GA) sample preparation uni.**MSU-**

4sample was dried in an oven set at 523 K for 24 hours. The sample was heated to 623 K at a rate of 1 K min^{-1} under vacuum ($5x10^{-3}$ mmHg) for five hours to degas them prior to the adsorption testing. CO_2 adsorption isotherms at 293 K were calculated using a static volumetric device. The volume of gas adsorbed per gram of adsorbent was calculated for adsorption capability at 293 K and 850 mmHg

2.10 References

1. Streib, W. E. Jordan, T. H. & Lipscomb, W. N. Single-crystal x-ray diffraction study of β nitrogen. *J. Chem. Phys.***37**, 2962–2965 (1962).
2. Sue, O. Ching, X. Nufretas, H. Chemical Crystallography Laboratory , Oxford. *Cell,* **2**. 1–23 (2010).
3. Sun, C. Zhou, D. Grant, D. J. W. & Young, V. G. Theophylline monohydrate. *Acta Crystallogr. Sect. E Struct. Reports Online***58**, 368–370 (2002).
4. Maarten Gérard Goesten, S. I. Crystal Engineering with Metal-Organic Frameworks. *Cryst. Growth Des*. **12**, 127 (2015).
5. Functionalities, A. & Recognition, N. Crystal Engineering of Metal - Organic Frameworks Containing Transformations , and Exchange Dynamics of Guests and Anions. *J. Appl. Crystallogr.***33**, 13–19 (2007).
6. Suresh, S., Jaisankar, V., Vinitha, G. & Kumar, R. M. Synthesis, structural, growth, optical, electrical, thermal and third order nonlinear optical properties of a organic single crystal: p -Toluidinium malonate. *J. Mol. Struct.***1202**, 123-133 (2020).
7. Krause, L., Herbst-Irmer, R., Sheldrick, G. M. & Stalke, D. Comparison of silver and molybdenum microfocus X-ray sources for single-crystal structure determination. *J. Appl. Crystallogr.***48**, 3–10 (2015).
8. McArdle, P. SORTX - a program for on-screen stick-model editing and autosorting of SHELX files for use on a PC . *J. Appl. Crystallogr.***28**, 65–65 (1995).
9. Chen, D. M., Xu, N., Qiu, X. H. & Cheng, P. Functionalization of metal-organic framework via mixed-ligand strategy for selective CO2 sorption at ambient conditions. *Cryst. Growth Des.***15**, 961–965 (2015).

10. Barbour, L. J. X-seed - A software tool for supramolecular crystallography. *J. Supramol. Chem.***1**, 189–191 (2011).

11. Spek, A. L. PLATON SQUEEZE: A tool for the calculation of the disordered solvent contribution to the calculated structure factors. *Acta Crystallogr. Sect. C Struct. Chem.***71**, 9–18 (2015).

12. Links, D. A. Syntheses , structures and properties of silver – organic frameworks constructed. *J. Appl. Crystallogr.* **4**, 10071–10081 (2011).

13. Escudero-Adán, E. C., Benet-Buchholz, J. & Ballester, P. The use of Mo Kα radiation in the assignment of the absolute configuration of light-atom molecules; The importance of high-resolution data. *Acta Crystallogr. Sect. B Struct. Sci. Cryst. Eng. Mater.***70**, 660–668 (2014).

Chapter 3

3.1 Introduction

In this chapter, a three-dimensional (3D) metal organic framework, MSU-3 with molecular formulae $[Ce_2(bpdc)_4(H_2O)_2]$ was prepared using 2,2'-bipyridine-5,5'-dicarboxylic acid and $Ce(NO_3)_3 \cdot 6H_2O$ as starting materials. The MOFs were characterised using X-Ray diffraction studies (SCXRD and PXRD), thermal analysis (TGA), spectroscopic analysis (FTIR) and electrochemical techniques (CV and EIS).

3.2 Synthesis of MSU-3 $[Ce_2(bpdc)_4(H_2O)_2]$

2,2'-bipyridine-5,5'-dicarboxylic acid (24.6 mg, 0.1007 mmol) was mixed with 10 mL DMF and preheated. To the clear solution was added $Ce(NO_3)_3 \cdot 6H_2O$ (88.1 mg, 0.203 mmol). The reaction mixture was stirred for 15 minutes and heated at 100 ^oC for 48 hours as shown in Scheme 3.1. After cooling the mixture to room temperature, the light-yellow block crystals were obtained in a good yield of 61%. The synthesised crystals were immersed in methanol for 24 hours to allow for the exchange of DMF with a low boiling point solvent. The active phase, **MSU-3a**, was then produced by heating the crystals under vacuum for 24 hours at a temperature of 160 ^oC.

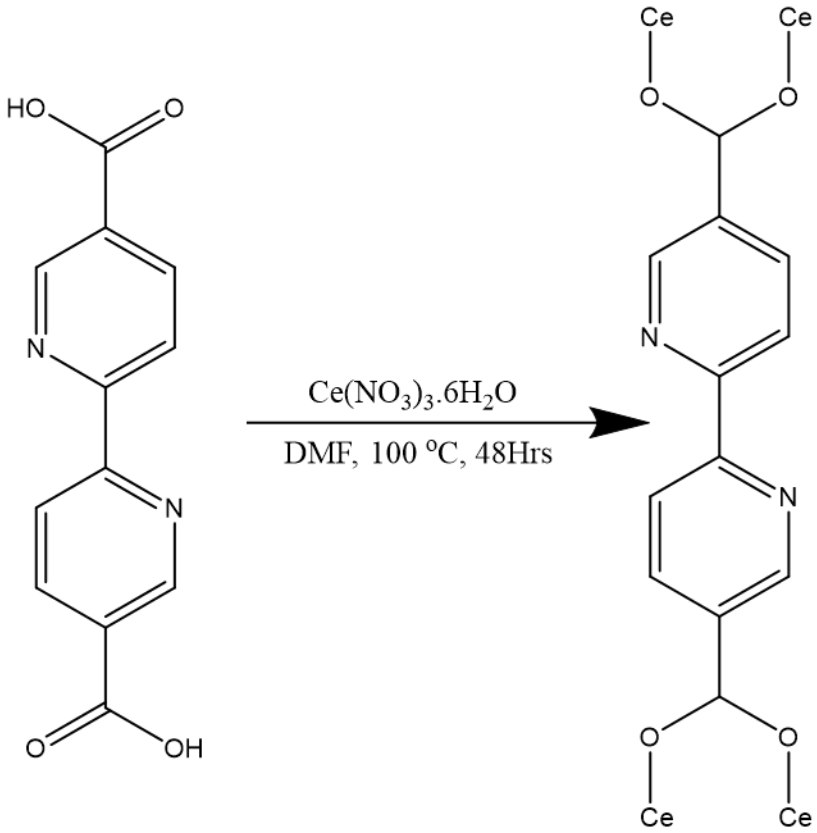

Scheme 3.1: Synthesis of MSU-3 illustrating the linker conformation and binding mode of the carboxylate moiety.

3.3 Synthesis of Ru(II)@MSU-3a

MSU-3 was soaked in methanol for 24 hours. It was activated at 160 ℃ so as to remove the DMF molecules incorporated within the pores for 24 hours so as to give **MSU-3a**. **MSU-3a** was cyclometalated using homogeneous system which is a direct method reported in literature. Stable cyclometalated ruthenium (II) complexes with $[RuCl_2(p\text{-cymene})]_2$ precursor, via the C–H bond deprotonation in the presence of sodium acetate at room temperature in methanol was produced. Thus, 50 mg of the activated crystalline powder was soaked in 10 mL of methanol with 27 mg sodium acetate and 49 mg of $[RuCl_2(p\text{-cymene})]_2$ for 24 h at room temperature to produce **Ru(II)@MSU-3a** shown in scheme 3.2.

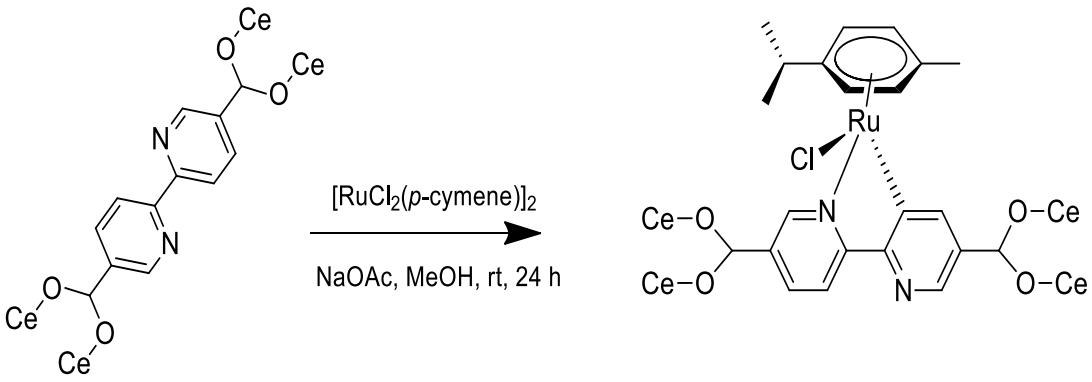

Scheme 3.2 Cyclometalation of the MOF backbone in **MSU-3a**

3.4 Single Crystal X-Ray Diffraction

Single crystal X-ray diffraction for MSU-3 was collected on a Bruker KAPPA APEX II DUO Diffractometer. Data collection was performed at low temperatures of 100(2) K. Unit cell refinement were performed using SAINT program[1]. Data was corrected for Lorentz-polarisation and absorption effects using the multi-scan method (SADABS)[2]. The program XPREP[3] was used to confirm the space group of the structures. The structure solutions were achieved by direct methods (program SHELXS)[4] and refined anisotropically by full-matrix least-squares on F^2 using SHELXL[5] within the X-SEED[6] interface.

The non-hydrogen atoms were located in the difference electron density maps and were refined anisotropically while all the hydrogen atoms were placed with geometric constraints, and refined with isotropic temperature factors. Some of the atoms in the DMF molecules were purified isotropically as a result of severe solvent disorder. There are restrictions on bond lengths and the thermal mobility of disordered groupings (DFIX)[5]. We noted the single crystal data for **MSU-3** is similar to what was being reported in the literature. For comparison's sake, the structure presented in literature

has been inclined in Table 3.1. Although the MOFs have similar unit cell parameters **MSU-3** has a large unit cell volume while the other parameters seem to be fairly comparable. The a and b-axis for the two MOFs are significantly different. Table 3.1 lists the crystallographic and refinement properties of the MOF found in literature and **MSU-3**.

Table 3.1: Crystallographic information and refinement parameters of Literature MOF and **MSU-3**

	Literature	**MSU-3**
Empirical formula	$C_{48}H_{48}Ce_2N_{10}O_{17}$	$C_{48}H_{28}Ce_2N_8O_{19}$
Formula weight ($gmol^{-1}$)	13170.21	946.54
Temperature/K	153(2)	100(2)
Crystal system	Monoclinic	Monoclinic
Space group	$P2_1/c$	*$P2_1/c$*
a (Å)	27.541(6)	26.4524(18)
b (Å)	11.126(2)	14.2180(11)
c (Å)	16.991(3)	17.0242(13)
α (deg)	90	90
β (deg)	99.01(3)	98.663(2)
γ (deg)	90	90
Volume ($Å^3$)	5142.2(18)	6329.8(8)
Calculated density (gcm^{-3})	1.701	3.564
Crystal size (mm^3)	0.140 x 0.160x 0.270	0.040 x 0.250 x 0.440
Radiation MoKα	(λ =0.88073)	(λ =0.71073)
2θ Max/°	31.25	28.31
Reflections collected	22398	296622
No. unique data	12324	9977
Final R indices	0.0922	0.1001
wR_2	0.2025	0.273
Goodness of fit	1.165	1.247
Highest different peak	3.597	1.012
Deepest hole	-2.203	-0.767

3.5 Structural Description

Single crystal X-ray diffraction revealed that **MSU-3** crystallises in a monoclinic system, with space group *P2₁/c*. The asymmetric unit contains two crystallographically independent Ce1 and Ce2 centres, four bpdc linkers and two bridging water molecules. The structure of **MSU-3** is made up of $Ce_2C_4O_8$ secondary building unit (SBU) rods which grow along the *c*-axis as shown in Figure 3.1a. The SBUs are connected by bpdc, linkers which grow along the *b*-axis to give a 3D structure. The presence of the bpdc linkers which connect the SBU along the *a-b* plane reduces void space found in **MSU-3.**

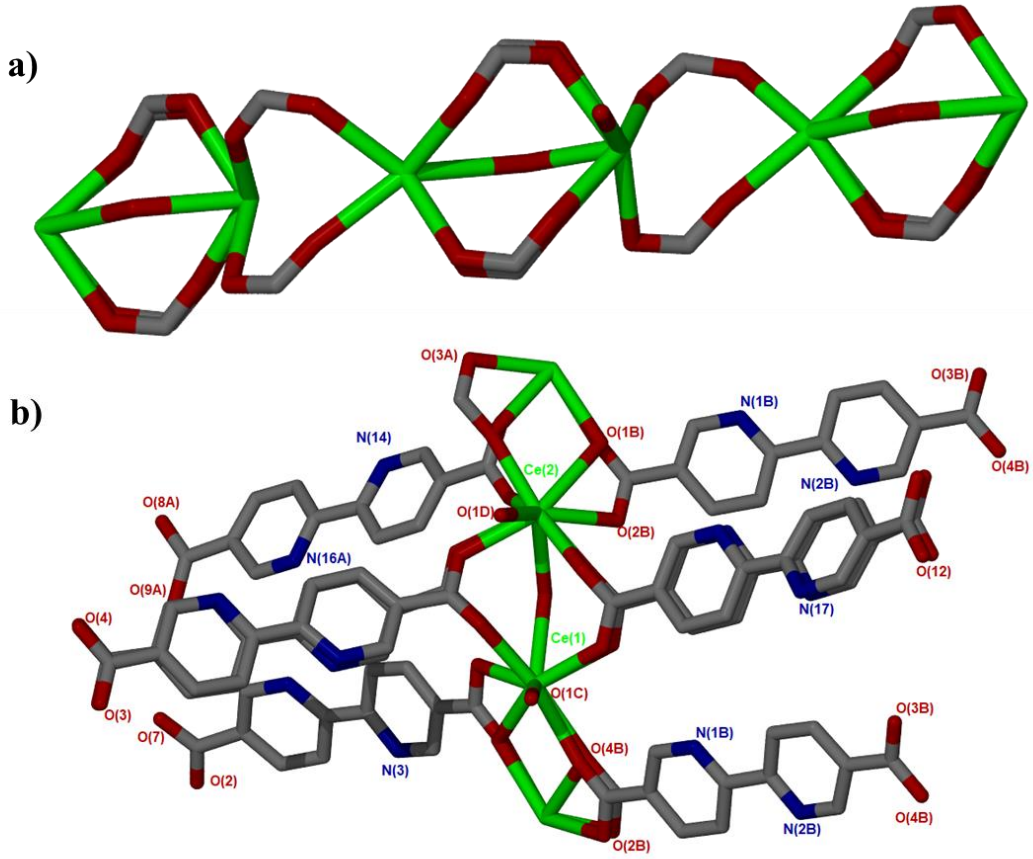

Figure 3.1: a) SBU rod generated *in situ*, b) Coordination environment around the two Ce^{III} metal centres modelled in the asymmetric unit.

Each Ce^{III} metal centre is coordinated to two water molecules and eight oxygen atoms of the bpdc linker and adopt a distorted CeO_8 square antiprismatic coordination geometry as illustrated in Figure 3.1b. Two of the coordinated linkers on each Ce^{III} metal centre was found to be disordered over two positions with 50% site occupancy. Due to disorder some non-hydrogen atoms were modelled isotropically.

The bpdc linker assumes a chelating mode connecting to the metal centre and a bridging mode connecting between the two metal centres. Both Ce^{III} metal centres are eight coordinated with Ce-O bond distances < 2.9 Å as shown in Table 3.2 and are consistent with literature reports. The solvent accessible volume calculated using PLATON[2] estimated at 16.4 %. The distances between the metal ions located at opposite sides of rhombs is 26.45 Å and the vertical distance is 15.37 Å as shown in Figure 3.2a. Packing diagram viewed along the c-axis drawn in a stick form as shown in figure 3.2b. The hydrogen atoms have been omitted for clarity.

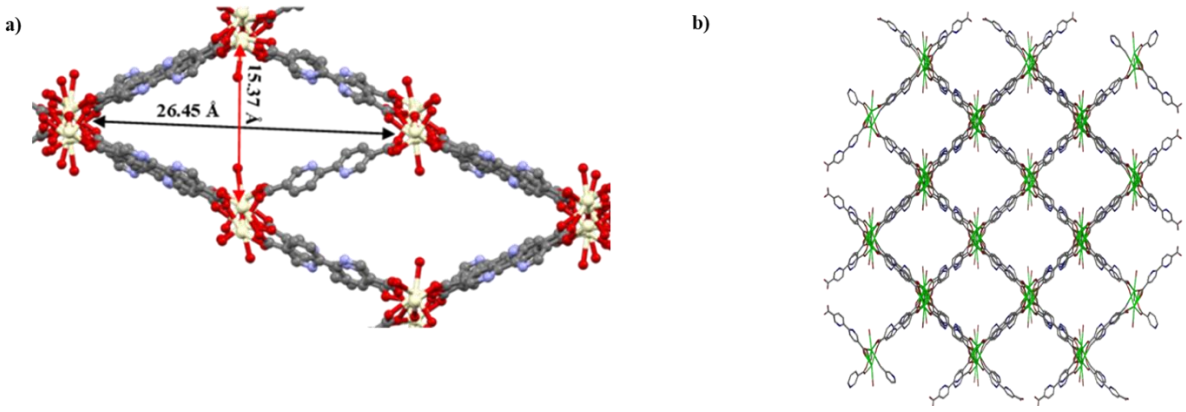

Figure 3.2: a) Schematic illustration of a rhombus shaped channel. b) Packing diagram in stick form. The hydrogen atoms have been omitted for clarity.

Table 3.2 Selected bond distances for MSU-3

Bond Type	Bond Length (Å)	Bond Type	Bond Length (Å)
Ce1-O3	2.988(7)	Ce2-O3	2.453(6)
Ce1-O6	2.488(7)	Ce2-O9	2.908(7)
Ce1-O7^{1}	2.479(6)	Ce2-O10	2.519(7)
Ce1-O8	2.455(7)	Ce2-O11	2.520(7)
Ce1-O9	2.471(6)	Ce2-O12^{4}	2.905(8)
Ce1-O12	2.612(7)	Ce2-O14^{3}	2.426(8)
Ce1-O13^{2}	2.405(7)	Ce2-O18^{5}	2.413(6)
Ce1-O17^{3}	2.516(7)	Ce2-O19	2.471(7)
Ce1-O1	2.515(9)	Ce2-O54	2.500(11)

Figure 3.3 illustrates the channels found in **MSU-3.** The analysis of cavities occupied by water and DMF molecules was done using the Mercury program.[7] These channels run along the c-axis.

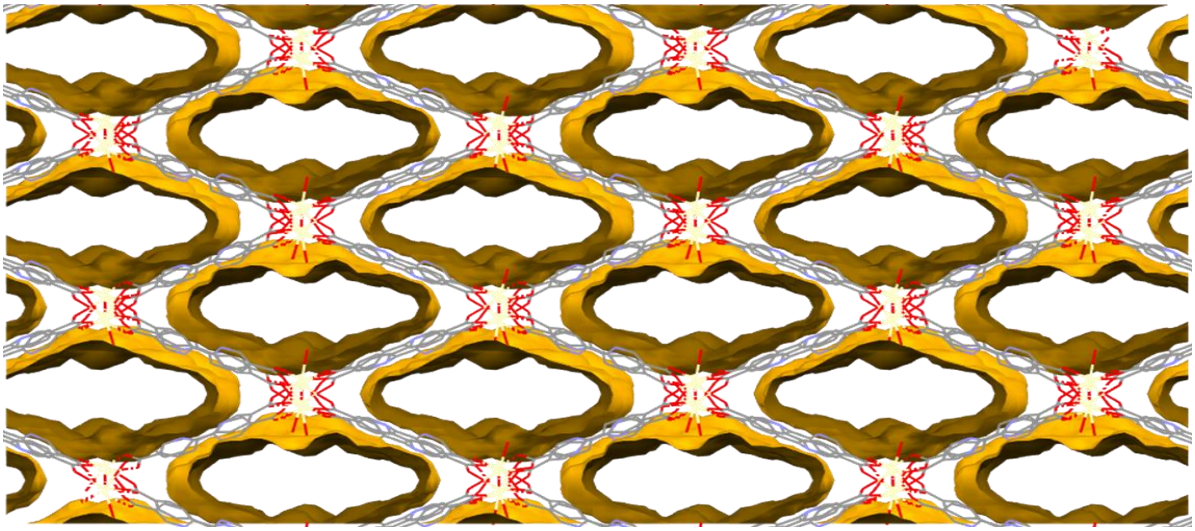

Figure 3.3 Cavities found in **MSU-3** in the absence of water and DMF molecules viewed along the c-axis. The outside and inside surfaces of the cavities are depicted in light and dark orange respectively.

3.6 Thermal Analysis

Thermogravimetric analysis of **MSU-3** (Figure 3.4) shows a 4.7 % weight loss between 100 and 200 ˚C, which is ascribed to the loss of two water molecules per formula unit (calculated 3.8%). The difference may be due to adsorbed moisture in the channels of **MSU-3**. From 200 ˚C, there is a plateau of up to 320 ˚C, an indication of high thermal stability. Decomposition of the framework occurs around 325 ˚C. **MSU-3** was activated by soaking the as-made crystals in methanol for 24 hours, followed by heating under vacuum for 24 hours at 160 ˚C to give **MSU-3a**. Complete removal of the solvent molecules was confirmed by TGA analysis which showed no weight loss until decomposition.

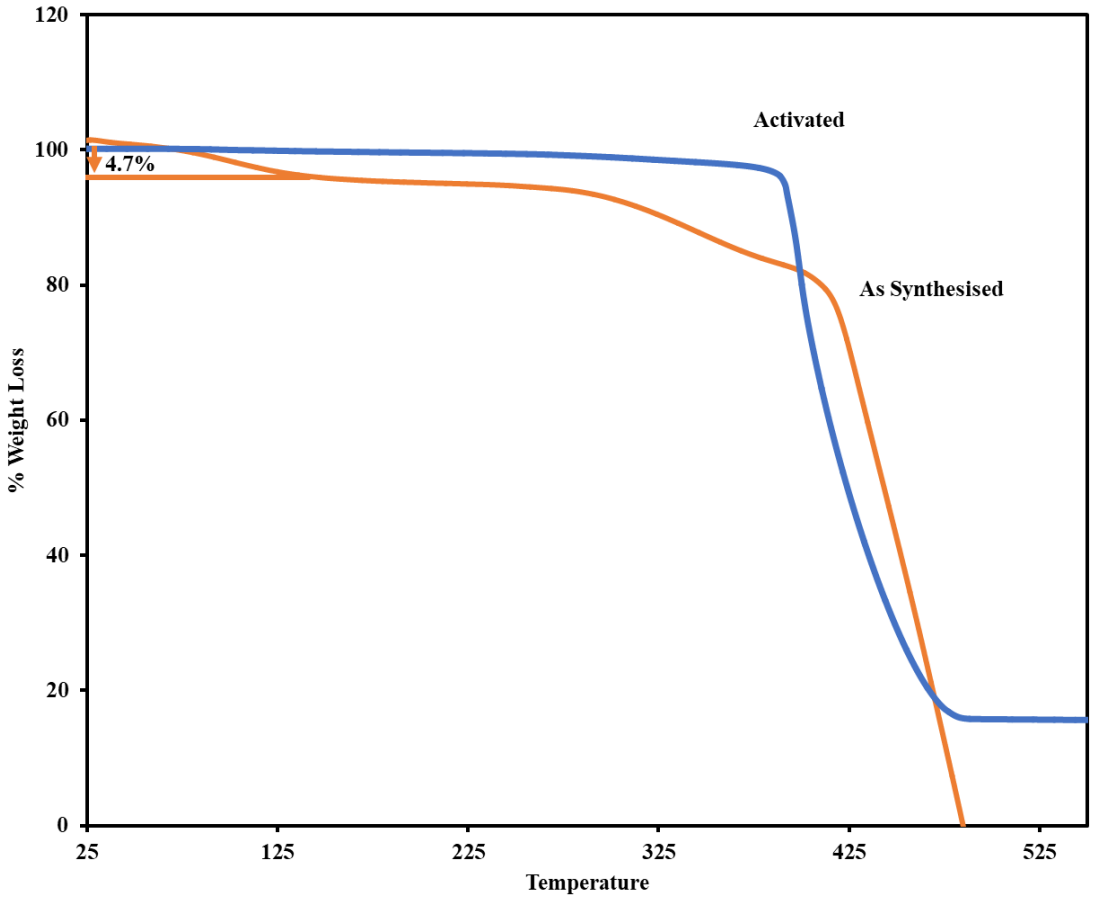

Figure 3.4: TGA traces of **MSU-3** and **MSU-3a**

3.7 FTIR Spectra Analysis

Fourier transform infrared (FTIR) spectroscopy is a technique used to obtain an infrared spectrum of absorption or emission of a solid, liquid or gas. The spectral data collected is analysed over a wide spectral range of 400 to 4000 cm^{-1} and the spectroscopy produces evidence whether the linker is coordinated to the metal centre. If the carboxylate functional groups are coordinated to the metal, a shift is expected in the absorption bands to a lower wavenumber as compared to the ligand. There is a shift of band 1681 cm^{-1} in the linker (COOH) to 1573 cm^{-1} in as synthesised and activated. This is evidence of coordination of Ce^{III} to the carboxylate moiety.

The asymmetric and symmetric carboxylate stretches in as synthesised are located at 1573 cm^{-1} and 1388 cm^{-1} respectively, and the magnitude of their separation was found to be 185 cm^{-1}, suggesting that the carboxylate group is coordinated to two Ce^{III} ions in a bidentate bridging fashion. The band located at 1527 cm^{-1} is attributed to the C-C of the benzene ring. Position does not change after activation and after cyclometallation (functionalised), suggesting that the binding mode of the carboxylate moiety is not affected. A broad peak at 3434 cm^{-1} assigned to methanol on the functionalised MOF is observed since methanol has been utilised as a solvent.

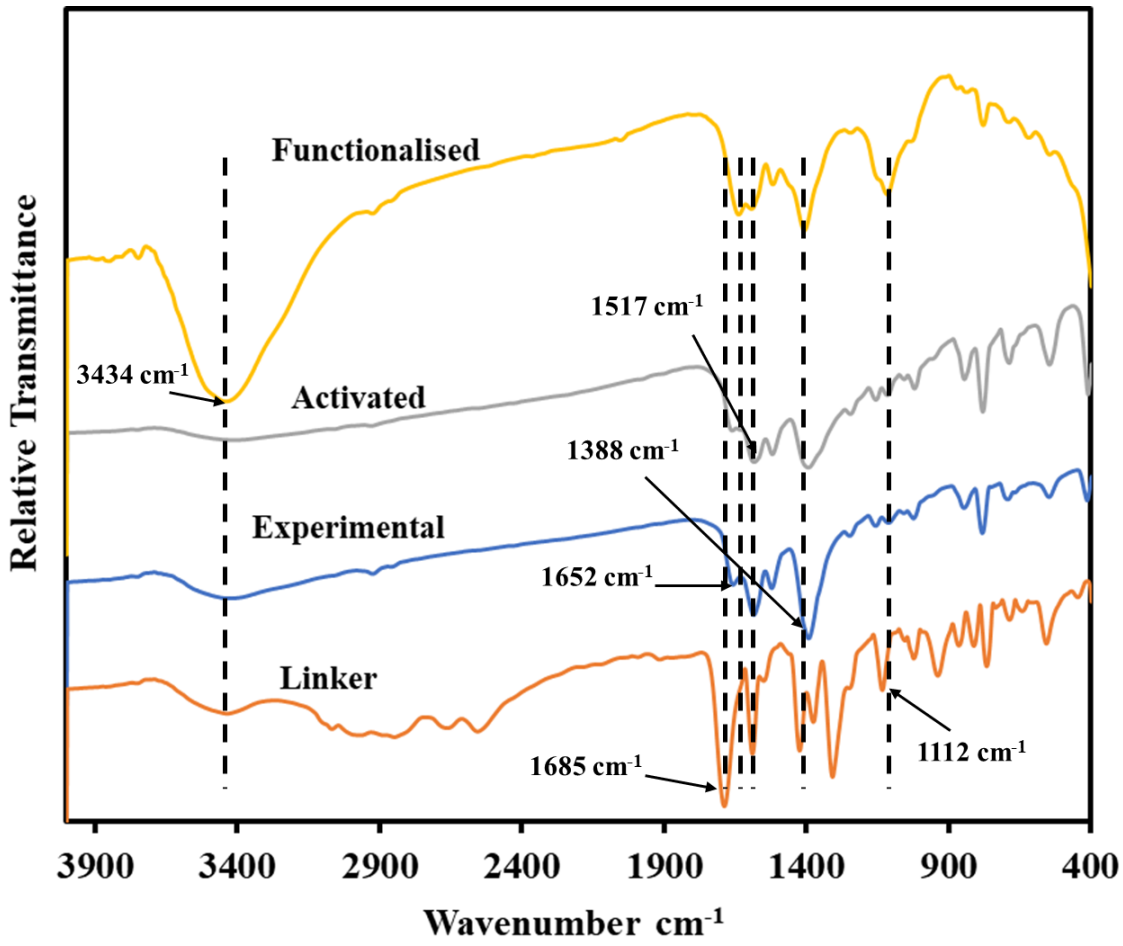

Figure 3.5: IR spectrum of the linker, experimental, activated and functionalized MOF.

3.8 PXRD Analysis

The phase purity of **MSU-3** was confirmed by a good match between experimental and calculated PXRD patterns (Figure 3.6). Comparison of the PXRD patterns of **as synthesised** and **activated** suggest the formation of a new phase upon activation. The structural integrity of MSU-3 is maintained upon cyclometalation of the MOF backbone as evidenced by a good match between the activated compounds, **MSU-3a** and the functionalised MOF, **Ru(II)@MSU-3a.**

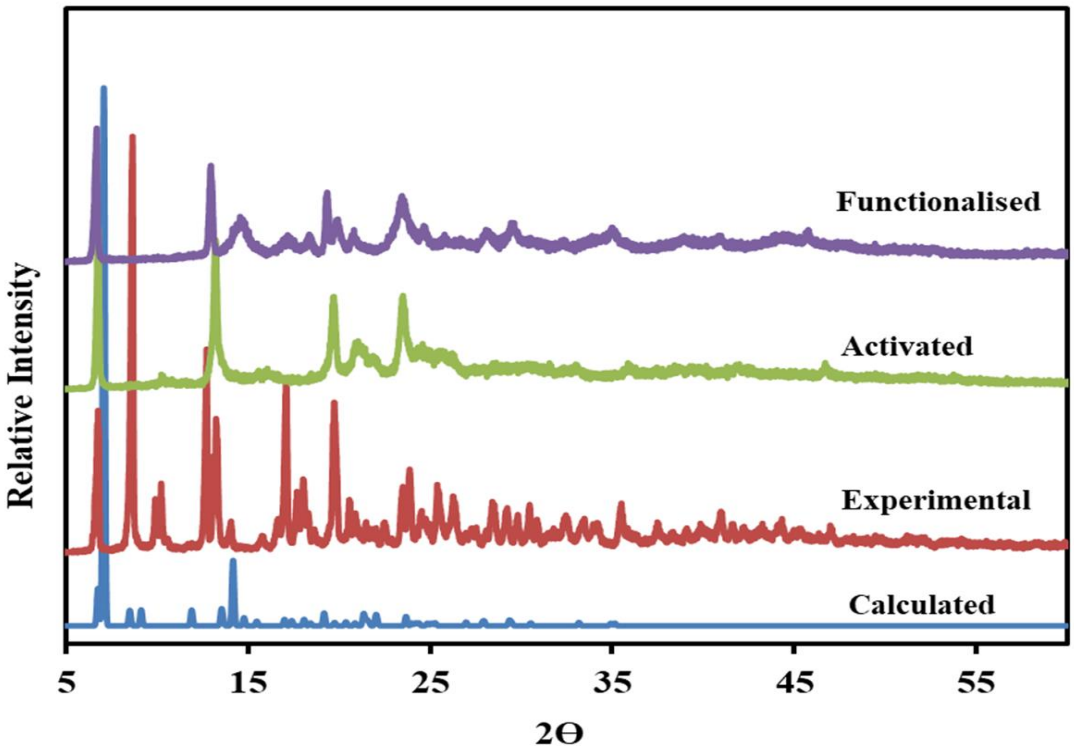

Figure 3.6: PXRD Patterns of **MSU-3** calculated**,** experimental, activated and functionalised**.**

3.9 SEM-EDX Studies

Scanning Electron Microscopy (SEM) illustrated in Fig 3.7, revealed that the surface morphology of is not affected during cyclometalation.

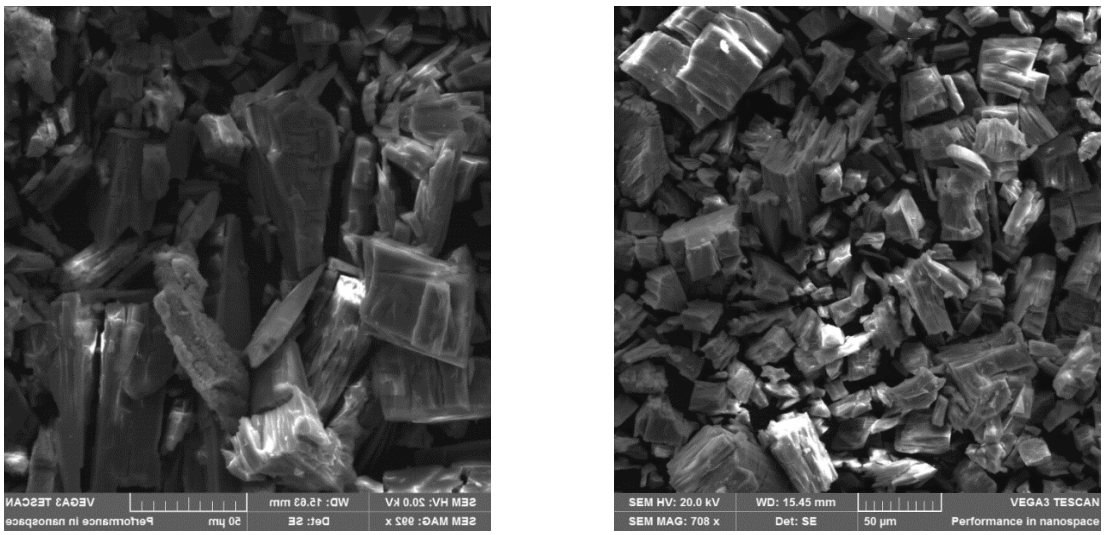

Figure 3.7. SEM analysis of Left: **MSU-3a** Right: **Ru(II)@MSU-3a**

Successful incorporation of ruthenium into the MOF was confirmed by SEM-EDS analysis which shows the presence of ruthenium and chlorine atoms with percentage weight of 0.7 % and 0.2 % respectively.

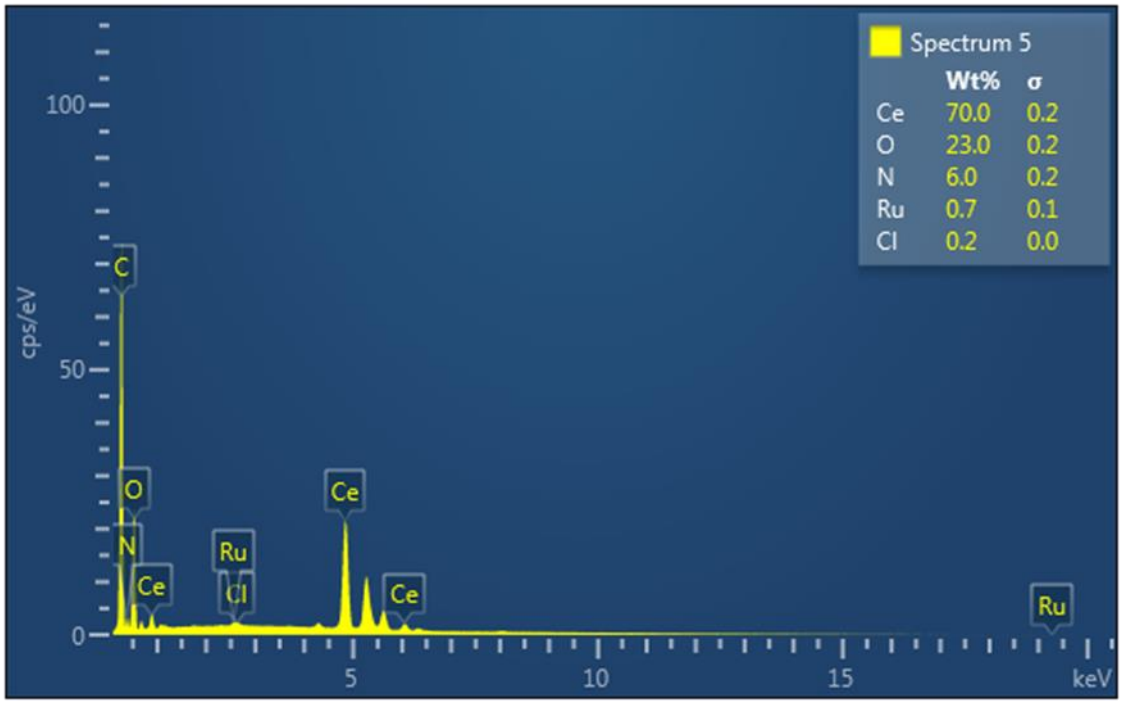

Figure 3.8. SEM-EDX analysis of **Ru(II)@MSU-3a** showing the presence of Ru and Cl atoms.

3.10 Chemical Stability Studies

A MOF is considered to be stable when it is able to resist the effects of exposure to various chemicals in the environment e.g. solvents, moisture, acids, bases and aqueous solutions containing coordinating anions.[8] The chemical weak points in most MOF structures are the metal-linker bonds. Thermodynamic stability of the MOFs usually correlates with the ability of the MOFs to preserve their structural integrity upon exposure to different operating environments. **MSU-3a** was soaked in different solvents for 24 hours to evaluate its chemical stability. Solvents used include

methanol, ethanol, tetrahydrofuran, triethylamine and water. PXRD studies in Figure 3.9 revealed that **MSU-3a** is poisoned by water as it provides proof of transformation from crystalline to an amorphous phase. In the presence of methanol, ethanol, tetrahydrofuran and triethylamine, **MSU-3a** revealed that it is highly stable as this can be seen from the patterns which have maintained their peak positions.

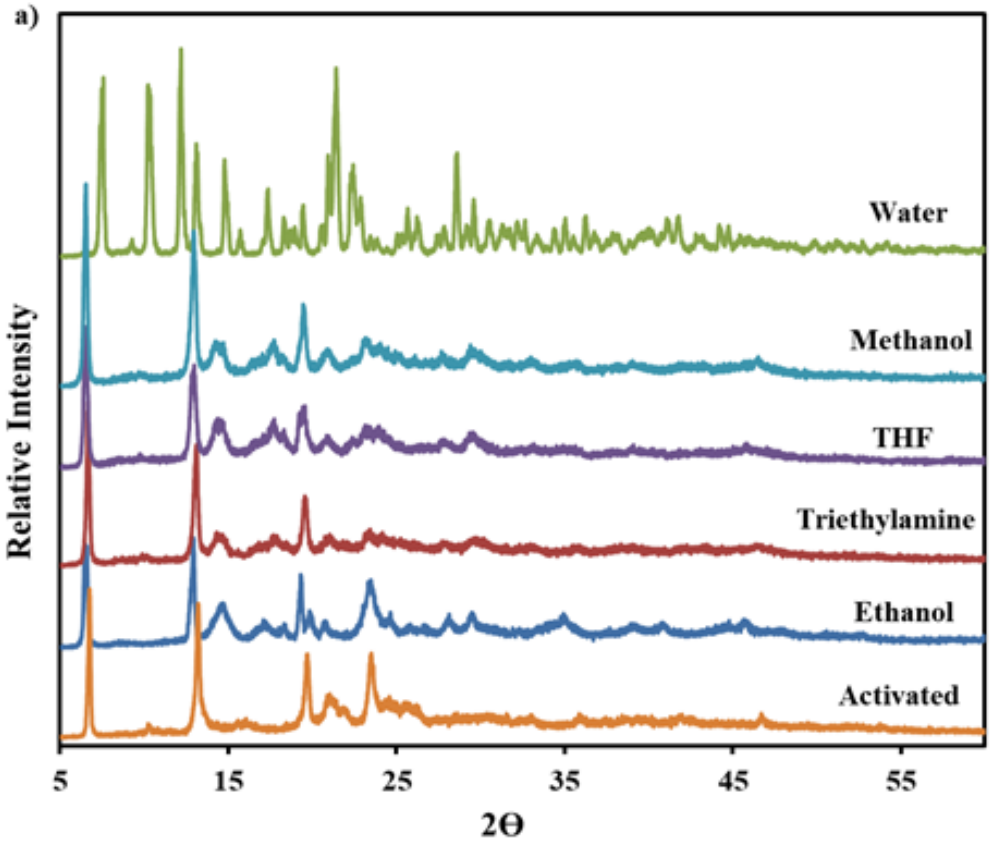

Figure 3.9 PXRD of **MSU-3a** soaked in different solvents for 24 hours.

3.11 Gas sorption Measurements

CO_2 sorption experiments were performed using a Micrometrics 3 Flex Surface Analyser. The samples were prepared by using a Micrometrics Flowprep with the low of nitrogen over the samples for 4 hours whilst heating at 60 °C. Furthermore, the

samples were heated at 150 °C under vacuum for 2 hours before the analysis commenced. CO_2 adsorption isotherm of **MSU-3a** in Figure 3.10 show a typical Type I isotherm suggesting microporosity nature of the material. **MSU-3a** has a volumetric uptake of 3.86 cm^3 (STP) g^{-1} (0.164799 $mmolg^{-1}$) and **Ru(II)@MSU-3a** has a volumetric uptake of 2.22 cm^3 (STP) g^{-1} (0.09487 $mmolg^{-1}$) at 293K. The pore volumes are relatively low, and the functionalised MOF has much lower volumetric uptake as compared to the activated MOF due to the partial occupancy by DMF molecules immobilised in the MOFs during synthesis. Interestingly, the amount of CO_2 uptake increased upon loading the MOF with Ru complex.

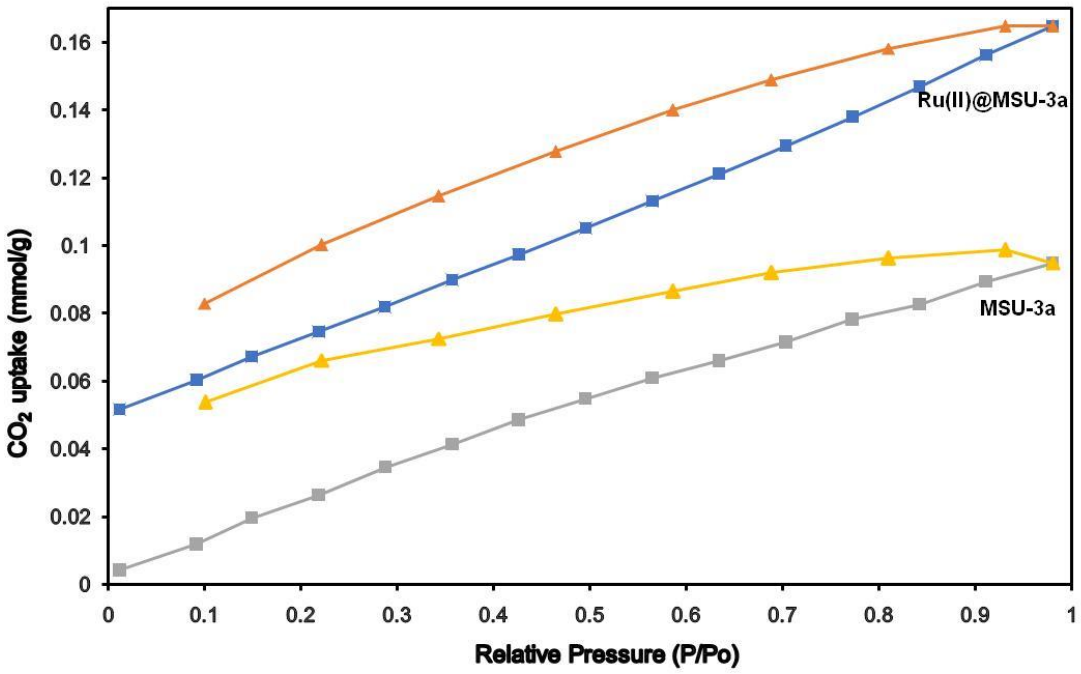

Figure 3.10: CO_2 adsorption-desorption isotherms for **MSU-3a**. Colour scheme orange; **MSU-3a desorbed**, blue; **MSU-3a adsorbed**, yellow; **Ru(II)@MSU-3a desorbed**, grey; **Ru(II)@MSU-3a adsorbed**.

3.12 Electrochemical Characterisation

Figure 3.11a shows voltammetric responses of the bare and modified GCE (**MSU-3**) in a 5 mM $[Fe(CN)_6]^{3-/4-}$ solution containing 0.1 M KCl at 100 mVs^{-1}. It can be seen that the peak current (I_p) of $[Fe(CN)_6]^{3-/4-}$ increased and the peak-to-peak separation (ΔEp) decreased in the order of bare electrode and **MSU-3** as it is shown in Table 3.3. To estimate the active area of MSU 3/GCE electrode, a solution of 5mM $[Fe(CN)_6]^{3-/4-}$ with 0.1 M KCl was used.

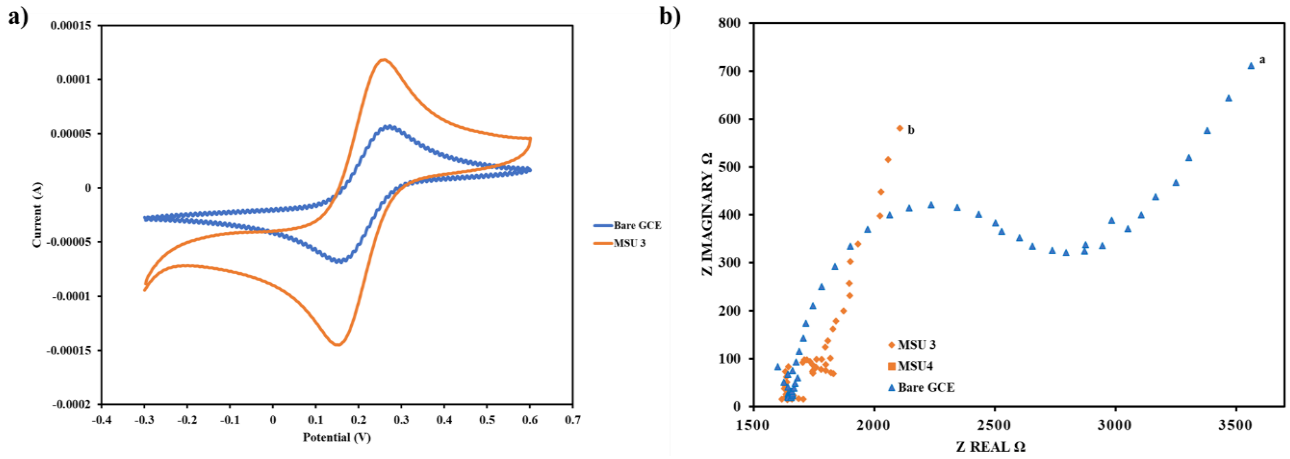

Figure 3.11: a) CVs of 5 mM $[Fe(CN)_6]^{3-/4-}$ at the bare GCE and **MSU-3** modified GCE electrode Scan rate 100 mVs^{-1} b) EIS of bare GCE and MSU-3 modified electrode in 5mM $[Fe(CN)_6]^{3-/4-}$ solution containing 0.1M KCl.

Table 3.3 Δ Ep and Ipa values of all working electrodes.

Electrode	Δ Ep values	Ipa
GCE	0.12	53 µA
MSU-3	0.088	109 µA

Figure 3.11b shows the Nyquist plots of bare GCE and MSU-3/GCE in 5 mM $[Fe(CN)_6]^{3-/4-}$ containing 0.1 M KCl, respectively. The MSU-3/GCE showed a lower interfacial electron transfer resistance (117±5Ω) than that of bare GCE (115±5Ω). This suggest that the electron transfer is faster at MSU-3/GCE than that of bare GCE, which facilitates the arrival of the electrochemical probe to the surface of the electrode.

3.13 Surface area determination

The surface area of GCE and MSU-3/GCE were determined using the $[Fe(CN)_6]^{3-/4-}$ redox system and applying Randles-Sevcik Equation (3.1).

$$I_p = (2.69 \times 10^5) n^{3/2} A D^{1/2} V^{1/2} C \qquad \textbf{Equation 3.1}$$

where D is the diffusion coefficient (7.6 × 10 -6 cm^2s^{-1}) and C the bulk concentration of the redox probe (5mM $[K_3Fe(CN)_6]$ in 0.1 M KCl), n is the number of electron transferred (n = 1) and A_{eff} is the effective surface area. The surface area of the modified electrode was found to be 0.57 cm^2 which was twice larger than the bare glassy carbon electrode area 0.0719 cm^2.

3.14 Summary

lanthanum based MOF **(MSU-3)**, with molecular formulae $[Ce_2(bpdc)_4(H_2O)_2]$ was synthesised using 2,2'-bipyridine-5,5'-dicarboxylic acid and $Ce(NO_3)_3{\cdot}6H_2O$ as starting materials. **MSU-3** crystallises in the monoclinic crystal system, space group *$P2_1/c$.* The overall structure is a three-dimensional (3D) structure. The activated phase of **MSU-3**, **MSU-3a**, was functionalised by cyclometallation of the MOF backbone using the metal precursor $[RuCl_2(p\text{-cymene})]_2$ to give **Ru(II)@MSU-3a**. PXRD analysis reveals a phase change induced by the inclusion of the [Ru(II)Cl(p-cymene)] in **MSU-**

3a. The stability experiments show that the carboxylate moiety's binding mode is preserved in various chemical conditions. The ability to capture CO_2 was assessed using the activated phases of **MSU-3**. At 293 K, **MSU-3** demonstrated noticeable carbon dioxide uptake. Electrochemical methods, i.e., cyclic voltammetry and electrochemical impedance spectroscopy were used to study the conductance of modified electrode, it showed very good electron transfer efficiency.

3.15 References

1. Suresh, S. Jaisankar, V. Vinitha, G. & Kumar, R. M. Synthesis, structural, growth, optical, electrical, thermal and third order nonlinear optical properties of a organic single crystal: p -Toluidinium malonate. *J. Mol. Struct.***1202**, (2020).
2. Krause, L. Herbst-Irmer, R. Sheldrick, G. M. & Stalke, D. Comparison of silver and molybdenum microfocus X-ray sources for single-crystal structure determination. *J. Appl. Crystallogr.***48**, 3–10 (2015).
3. Sabouni, R., Kazemian, H. & Rohani, S. Carbon dioxide capturing technologies: A review focusing on metal organic framework materials (MOFs). *Environ. Sci. Pollut. Res.***21**, 5427–5449 (2014).
4. McArdle, P. SORTX - a program for on-screen stick-model editing and autosorting of SHELX files for use on a PC . *J. Appl. Crystallogr.***28**, 65–65 (1995).
5. Spek, A. L. PLATON SQUEEZE: A tool for the calculation of the disordered solvent contribution to the calculated structure factors. *Acta Crystallogr. Sect. C Struct. Chem.***71**, 9–18 (2015).
6. Barbour, L. J. X-seed - A software tool for supramolecular crystallography. *J. Supramol. Chem.***1**, 189–191 (2001).
7. C. F. Macrae, I. Sovago, S. J. Cottrell, P. T. A. Galek, P. McCabe, E. P. & M. Platings, G. P. Shields, J. S. Stevens, M. T. and P. A. W. The Genesis of the C. P. A. Movement. *J. Appl. Cryst.* **19**, 226–235 (2020)
8. Ding, M., Cai, X. & Jiang, H. L. Improving MOF stability: Approaches and applications. *Chem. Sci.***10**, 10209–10230 (2019).

Chapter 4

4.1 Introduction

In this chapter, a three-dimensional (3D) metal organic framework, **MSU-4** with molecular formulae $[Ce(H_2O)_2(bpdc)_{3/2}(DMF)\cdot 7(DMF)]$ was prepared using 2,2'-bipyridine-5,5'-dicarboxylic acid and $Ce(NO_3)_3\cdot 6H_2O$ as starting materials. The MOFs were characterised using X-Ray diffraction studies (SCXRD and PXRD), thermal analysis (TGA), spectroscopic analysis (FTIR) and electrochemical techniques (CV and EIS).

4.2 Synthesis of MSU-4

2,2'-bipyridine-5,5'-dicarboxylic acid (12.1 mg, 0.0495 mmol) was mixed with 10 mL DMF and preheated. To the clear solution was added $Ce(NO_3)_3\cdot 6H_2O$ (44.8 mg, 0.1031 mmol). The reaction mixture was stirred for 15 minutes and was heated to 65 ^oC for 72hours (Scheme 4.1). After cooling the mixture to room temperature, the light-yellow block crystals were obtained in a fair yield of 48%. The as synthesised crystals were immersed in methanol for 24 hours to allow for the exchange of DMF with a low boiling point solvent, which activated **MSU-4**. The active phase, **MSU-4a**, was then produced by heating the crystals under vacuum for 24 hours at a temperature of 160 ^oC.

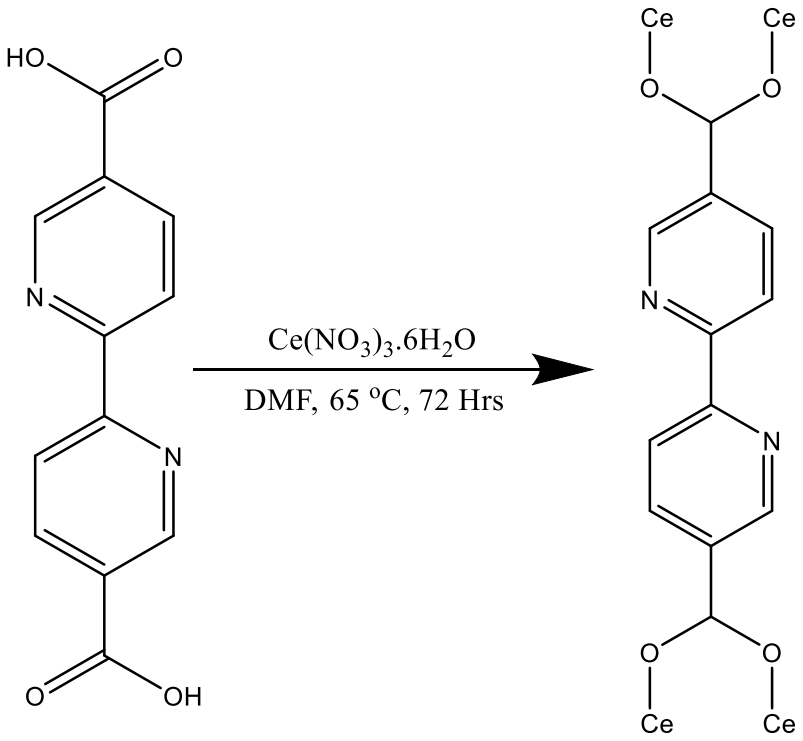

Scheme 4.1: Synthesis of **MSU-4** illustrating the linker conformation and binding mode of the carboxylate moiety.

4.3 Synthesis of Ru(II)@MSU-4a

MSU-4 was soaked in methanol for 24 hours. It was activated at 160 ℃ to remove the DMF molecules incorporated within the pores for 24 hours so as to give **MSU-4a**. **MSU-4a** was cyclometalated using homogeneous system which is a direct method reported in literature. Stable cyclometalated ruthenium (II) complexes with $[RuCl_2(p\text{-cymene})]_2$ precursor, via the C–H bond deprotonation in the presence of sodium acetate at room temperature in methanol was produced. Thus, 50 mg of the activated crystalline powder was soaked in 10 mL of methanol with 27 mg sodium acetate and 49 mg of $[RuCl_2(p\text{-cymene})]_2$ for 24 h at room temperature to produce **Ru(II)@MSU-4a** shown in scheme 4.2.

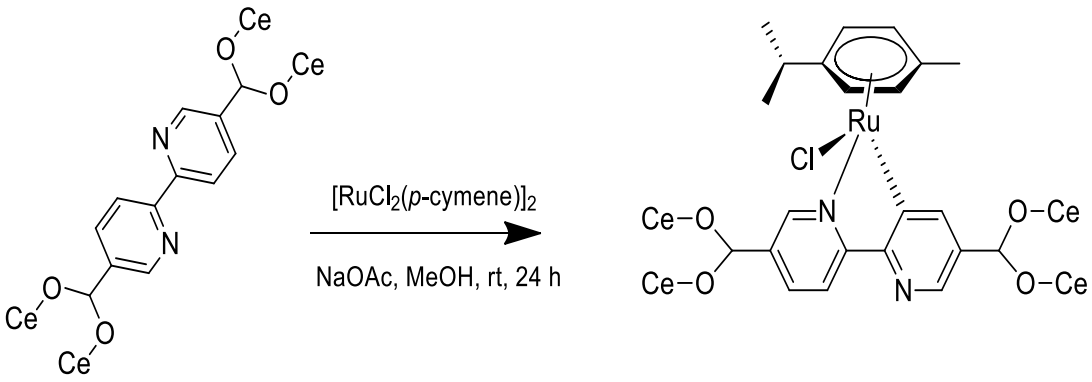

Scheme 4.2 Cyclometalation of the MOF backbone in **MSU-4a**

4.4 Single Crystal X-Ray Diffraction

On a Bruker KAPPA APEX II DUO Diffractometer, **MSU-4** single crystal X-ray diffraction data was collected. Data collections was performed at low temperatures of 100(2) K. Unit cell refinement were performed using SAINT program[1]. Data was corrected for Lorentz-polarisation and absorption effects using the multi-scan method (SADABS)[2]. The program XPREP[3] was used to confirm the space group of the structures. The structure solutions were achieved by direct methods (program SHELXS)[4] and refined anisotropically by full-matrix least-squares on F^2 using SHELXL[5] within the X-SEED[6] interface. Geometric restrictions were used to position hydrogen atoms, and isotropic temperature factors were used to refine them. Some of the atoms in the DMF molecules were purified isotropically as a result of severe solvent disorder. There are restrictions on bond lengths and the thermal mobility of disordered groupings (DFIX). Table 4.1 lists the **MSU-4**'s crystallographic and refinement properties.

Table 4.1: Crystallographic information and refinement parameters of **MSU-4**

	MSU-4
Empirical formula	$C_{42}H_{55}CeN_{11}O_{16}$
Formula weight ($gmol^{-1}$)	1110.08
Temperature/K	100(2)
Crystal system	Triclinic
Space group	*P-1*
a (Å)	9.6470(4)
b (Å)	12.6708(5)
c (Å)	14.8570(5)
α (deg)	108.0680(12)
β (deg)	103.5500(11)
γ (deg)	106.3352(13)
Volume ($Å^3$)	1550.51(16)
Calculated density (gcm^{-3})	1.604
Crystal size (mm^3)	0.050 x 0.150 x 0.160
Radiation MoKα	(λ =0.71073)
2θ Max/°	28.73
Reflections collected	143634
No. unique data	9220
Final R indices	0.0393
wR_2	0.0986
Goodness of fit	1.056
Highest different peak	2.308
Deepest hole	-1.583

4.5 Structural Description

Single crystal X-ray diffraction revealed that **MSU-4** crystallises in a triclinic system with, space group *P-1*. The asymmetric unit contains one Ce1 centre attached to one and a half bpdc linkers, one coordinated and seven solvated DMF molecules. The structure of **MSU-4** is made up of $Ce_2C_2O_4$ secondary building unit (SBU) rods which grow along the *a*-axis as shown in Figure 4.1a. The SBUs are connected by bpdc, linkers which grow along the *c*-axis to give a 3D structure. The presence of the bpdc

linkers which connect the SBU along the *b*-*c* plane reduces void space found in **MSU-4.**

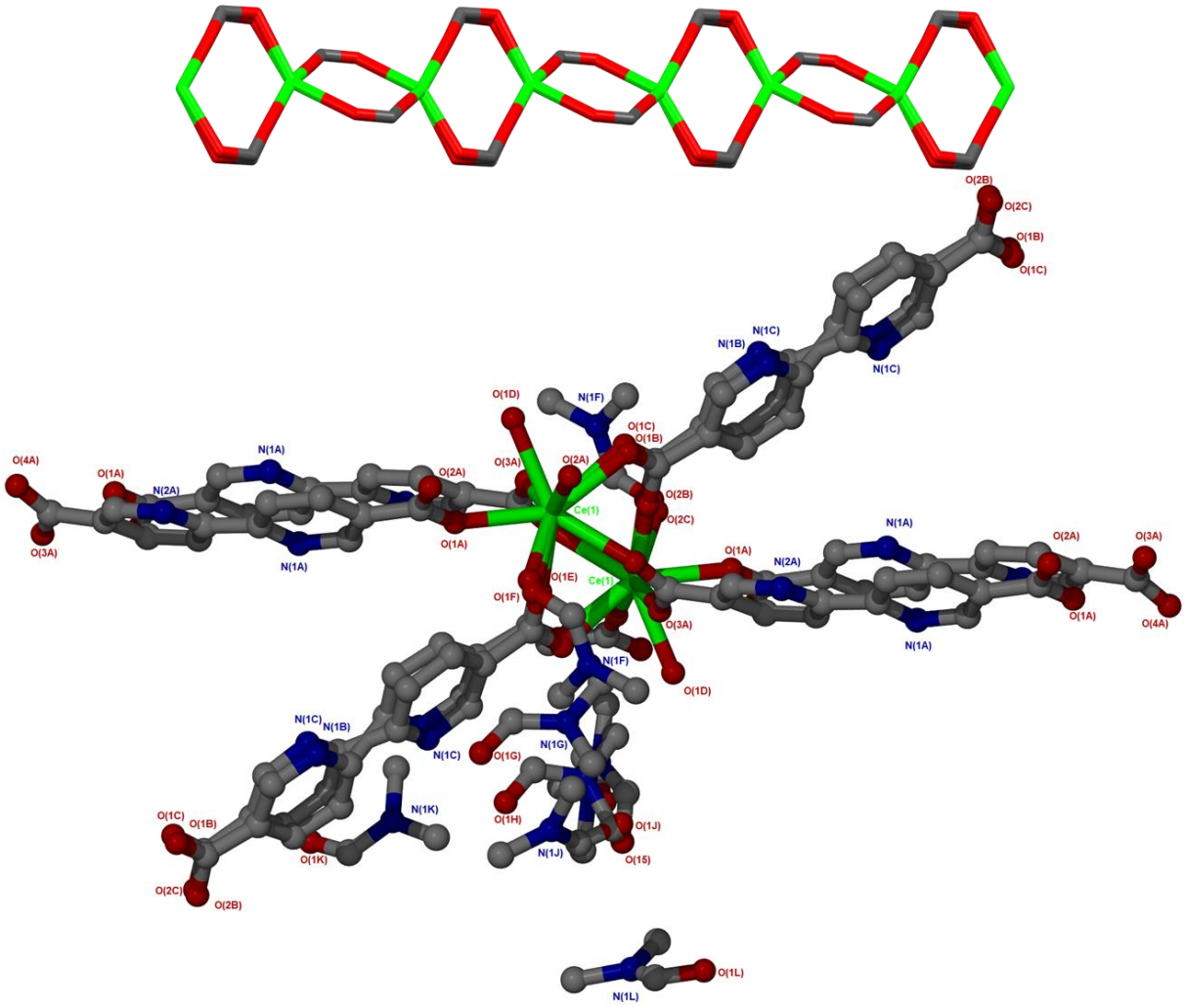

Figure 4.1: a) SBU rod generated *in situ*, b) Coordination environment around the Ce^{III} metal centre modelled in the asymmetric unit.

The Ce^{III} metal centre is coordinated to six oxygen atoms of the bpdc linker to furnish a square antiprismatic geometry, formed by six oxygen O atoms (Ce-O bond distances < 2.9 Å) as illustrated in Figure 4.1b. Two of the coordinated linkers around the Ce^{III} metal centre was found to be disordered over two positions. Due to disorder some

non-hydrogen atoms were modelled isotropically. The bond angle around Ce^{III} metal centre range from 69.1(2)º to 147.85(17)º.

The solvent accessible volume in the absence of solvent molecules is 51.6 % as estimated by PLATON. Packing diagrams viewed along the c-axis drawn in van der Waals radii are shown in Figure 4.2a. The distances between the metal ions located at opposite sides is 12.67 Å and the vertical distance is 26.57 Å as shown in Figure 4.2b. The hydrogen atoms have been omitted for clarity.

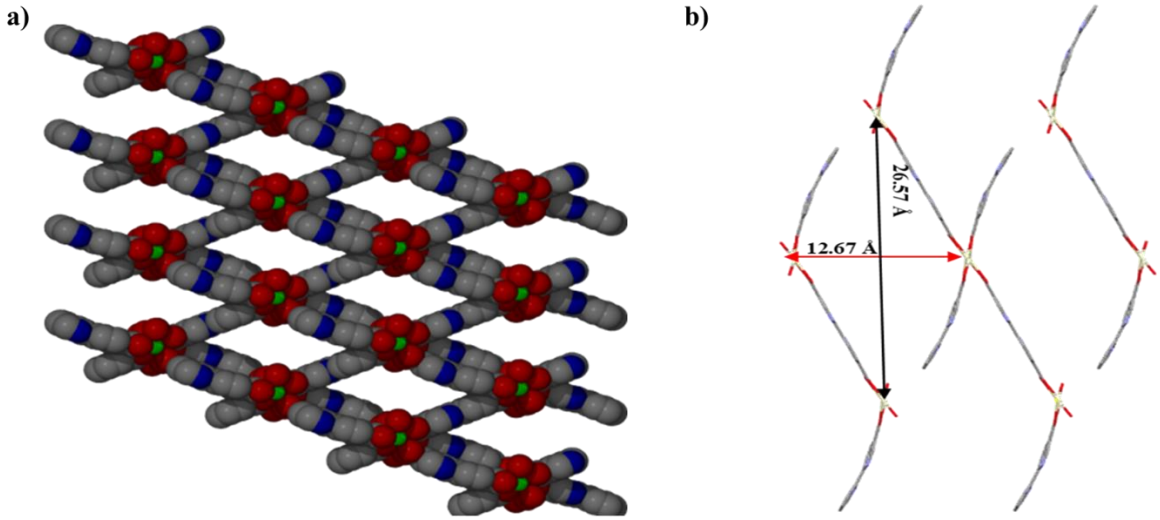

Figure 4.2: a) Channels of **MSU-4** viewed along the a-axis in van der Waals radii b) Packing diagram in stick form. The hydrogen atoms have been omitted for clarity.

Table 4.2 Selected bond distances for MSU-4

Bond Type	Bond Length (Å)
Ce1-O1	2.472(10)
Ce1-O2	2.452(10)
Ce1-O7	2.535(10)
Ce1-O5	2.429(10)
Ce1-O8	2.546(10)
Ce1-O4	2.399(10)
Ce1-O31	2.388(10)
Ce1-O62	2.380(10)

Figure 4.4 illustrates the channels found in **MSU-4.** The analysis of cavities occupied by DMF using the Mercury program[7] shows that they are interconnected as illustrated in Figure 4.4.

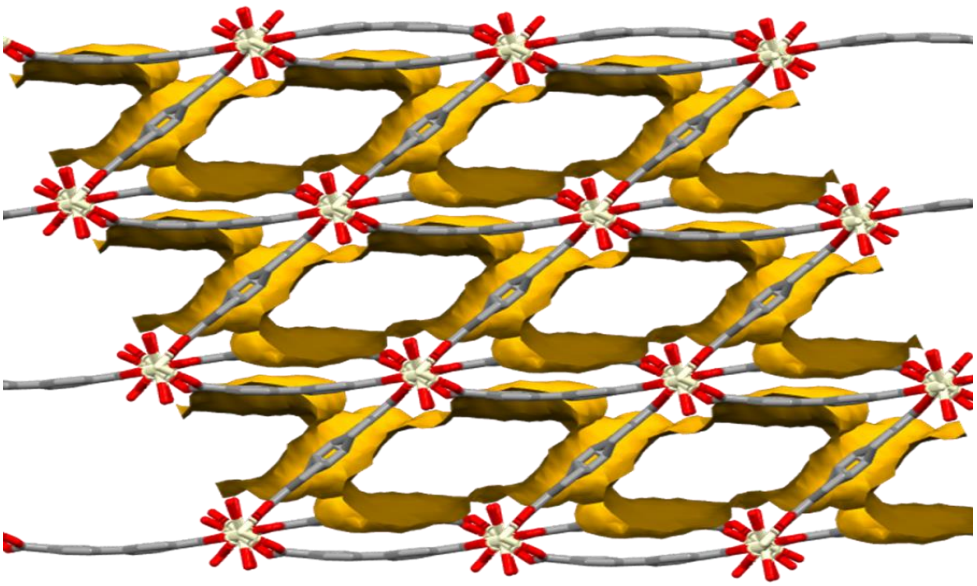

Figure 4.4 Cavities found in **MSU-4** in the absence of DMF viewed along the a-axis. The outside and inside surfaces of the cavities are depicted in light and dark orange respectively

4.6 Thermal analysis

Thermogravimetric analysis of **MSU-4** (Figure 4.5) shows a 61.5 % weight loss between 25 and 80 ˚C, which is ascribed to the loss of eight DMF molecules per formula unit modelled in the structure of **MSU-4** (calculated 61.1 %). From 100 ˚C, there is a plateau up to 370 ˚C, an indication of high thermal stability. Decomposition of the framework occurs around 380 ˚C. **MSU-4** was activated by soaking the as-made crystals in methanol for 24 hours, followed by heating under vacuum for 24 hours at 160 ˚C to give **MSU-4a**. Complete removal of the solvent molecules was confirmed by TGA analysis which showed no weight loss until decomposition.

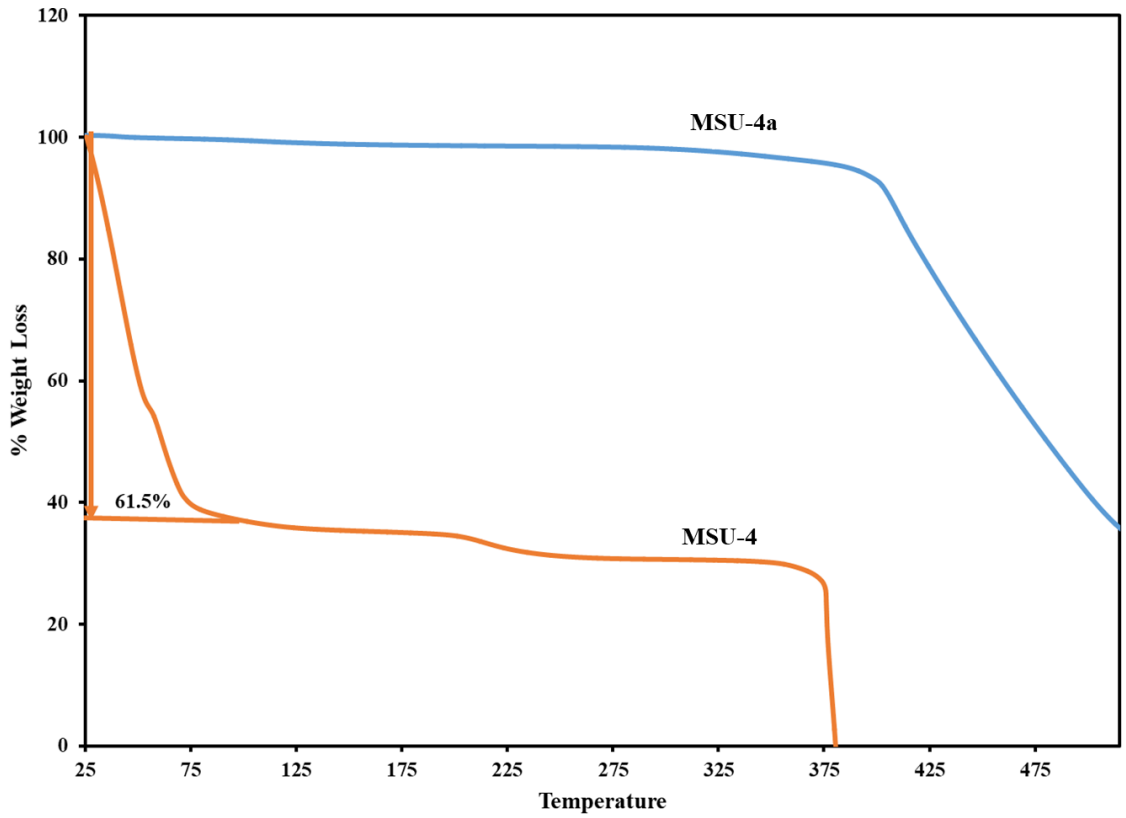

Figure 4.5: TGA traces of **MSU-4** and **MSU-4a**.

4.7 FTIR Spectra Analysis

There is a shift of band 1681.93 cm^{-1} in the linker (COOH) to 1566 cm^{-1} in as synthesised and activated. This is evidence of coordination of Ce^{III} to the carboxylate moiety. Successful activation of **MSU-4** is evidenced by the disappearance of the absorption band at 1658 cm^{-1}, which is attributed to co-ordinated DMF molecules. The asymmetric and symmetric carboxylate stretches in as synthesised are located at 1566 cm^{-1} and 1396 cm^{-1} respectively, and the magnitude of their separation was found to be 170 cm^{-1}. This suggests that the carboxylate group is coordinated to two Ce^{III} ions in a bidentate bridging fashion. The band located at 1519 cm^{-1} is attributed to the C-C of the benzene ring. Position does not change after activation, suggesting

that the binding mode of the carboxylate moiety is not altered. A broad peak at 3430 cm^{-1} is observed indicating presence of moisture.

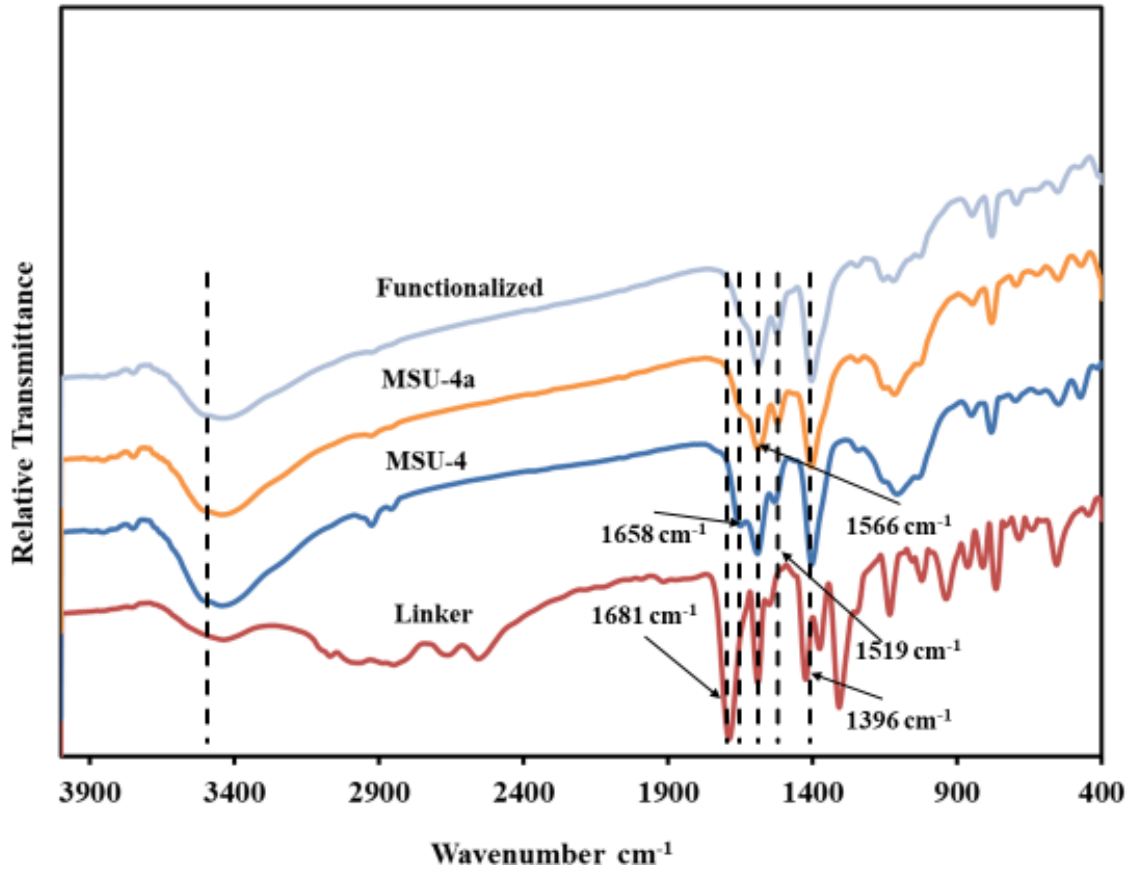

Figure 4.6: IR spectrum of the **linker**, **MSU-4, MSU-4a, and Functionalized.**

4.8 PXRD Analysis

The phase purity of **MSU-4** was confirmed by a good match between the experimental and calculated PXRD patterns (Figure 4.7). Comparison of the PXRD patterns of **MSU-4** and **MSU-4a** suggest the formation of a new phase upon activation. The functionalised matches well with the activated suggesting the structural integrity is maintained after functionalisation.

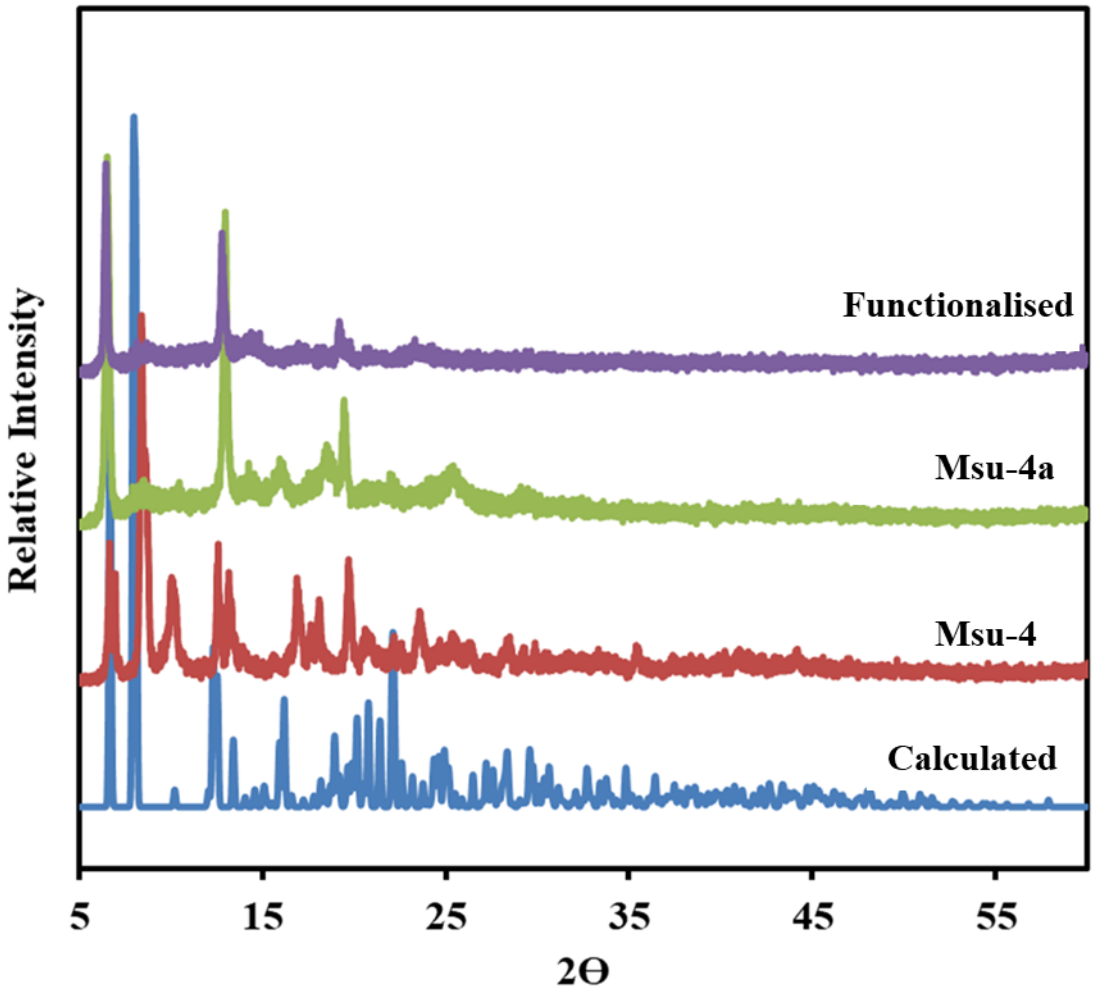

Figure 4.7: PXRD Patterns of **MSU-4** calculated**,** as synthesised, activated and functionalised**.**

4.9 SEM-EDX Studies

SEM (Figure 4.8) revealed that the surface morphology of the MOF is also not affected during cyclometalation.

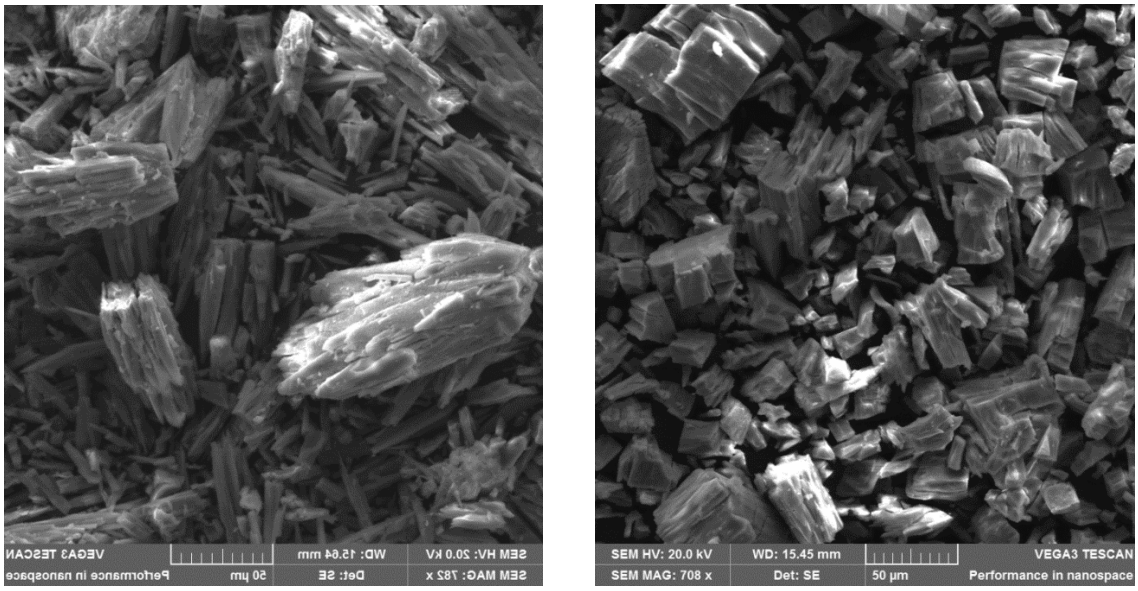

Figure 4.8 SEM analysis Left: **MSU-4a** Right: **Ru(II)@MSU-4a**

Successful incorporation of ruthenium into the MOF was also confirmed by SEM-EDS analysis (Figure. 4.9), which shows the presence of ruthenium and chlorine atoms with percentage weight of 1.6 % and 0.7 % respectively.

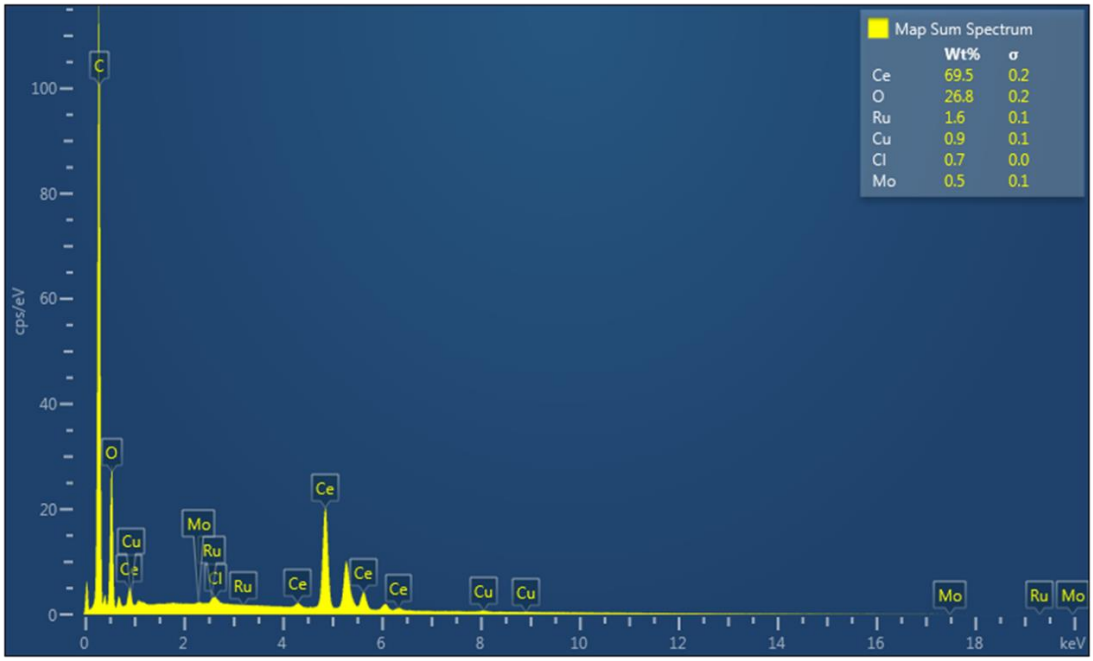

Figure 4.9. SEM-EDX analysis of **Ru(II)@MSU-4a** showing the presence of Ru and Cl atoms.

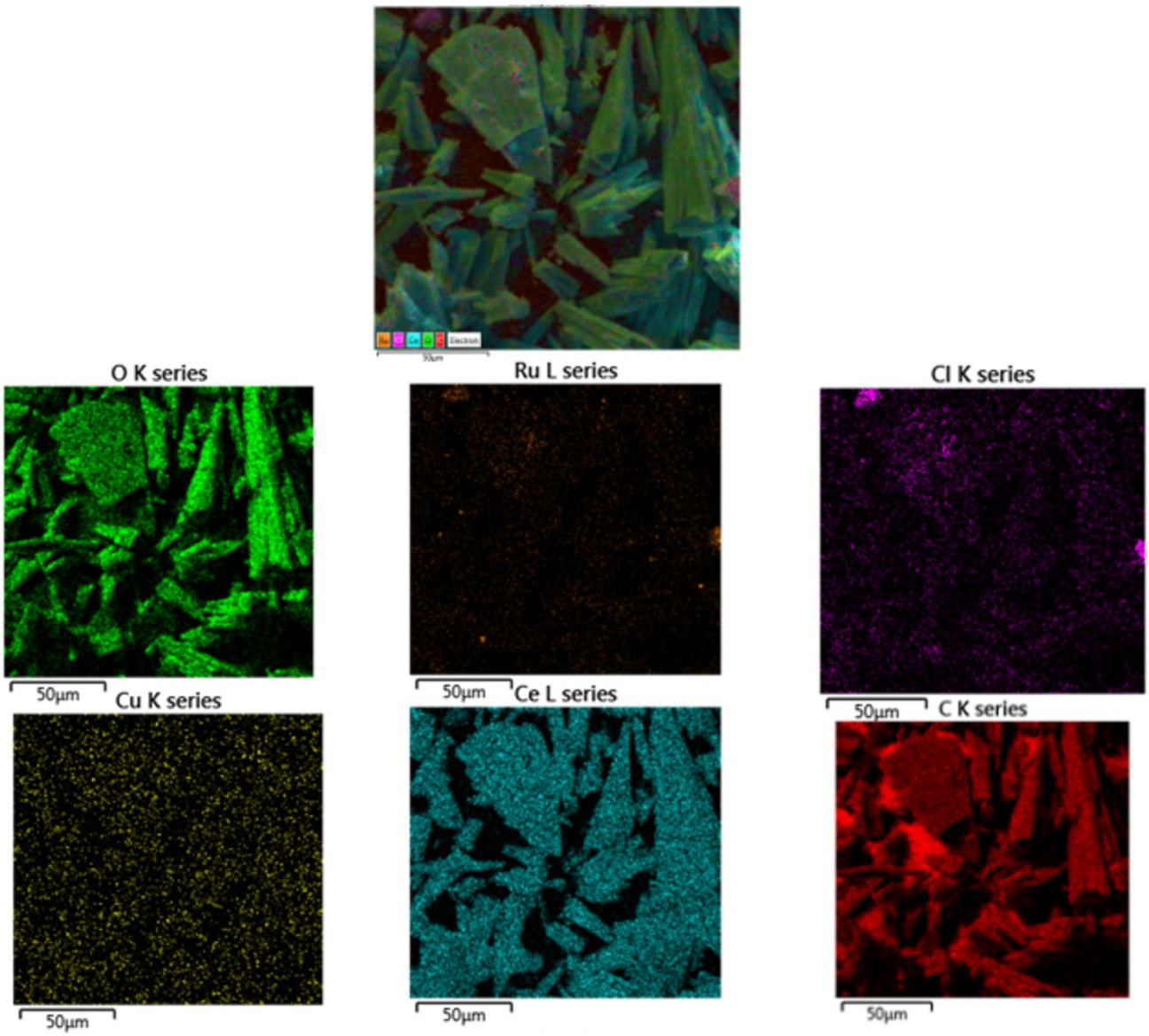

Figure 4.10 a) SEM images and **b) elemental mapping** of **Ru(II)@MSU-4a**

An image showing the spatial distribution of elements in a sample is called an element map. Element maps are extremely useful for displaying element distributors in textural context, particularly for showing compositional zonation. Elemental mapping of EDX for individual atoms in **Ru(II)@MSU-4a** in Figure 4.10b. Infers a consistent and even distribution of Ru(II) throughout the matrix.

4.10 Chemical Stabilities Studies

The chemical stability of **MSU-4** was verified by comparing the PXRD pattern of a MOF before and after soaking in different chemical solutions. PXRD analysis after the exposure to these reaction conditions revealed details about the integrity of the crystal structure as shown in Figure 4.11.

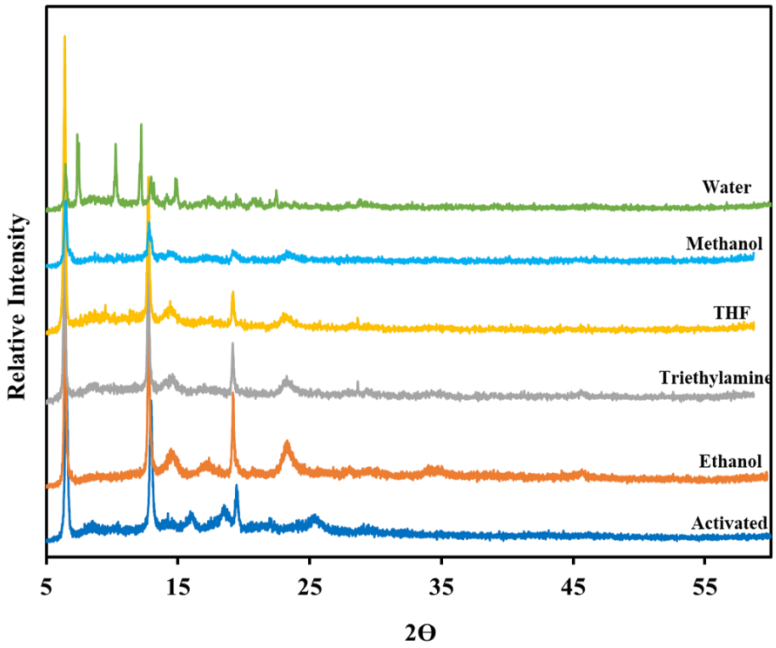

Figure 4.11: PXRD of **MSU-4a** soaked in different solvents for 24 hours.

As shown in Figure 4.11 pattern of the recovered samples, **MSU-4a** is stable in most solvents except water where we can see formation of a new phase.

4.11 Gas sorption Measurements

CO_2 sorption experiments were performed using a Micrometric Smart VacPrep060 Analyser. The samples were prepared by using a Micrometrics Smart VacPrep060 (Norcross, GA) sample preparation uni with the low of nitrogen over the samples for 5 hours whilst heating at 60 °C. Furthermore, the samples were heated at 150 °C

under vacuum for 2 hours before the analysis commenced. CO_2 adsorption isotherm of **MSU-4a** in Figure 4.12 show a typical Type I isotherm suggesting microporosity nature of the material. **MSU-4a** has a volumetric uptake of 4.44 cm^3 (STP) g^{-1} (0.19 $mmolg^{-1}$) at 293K.

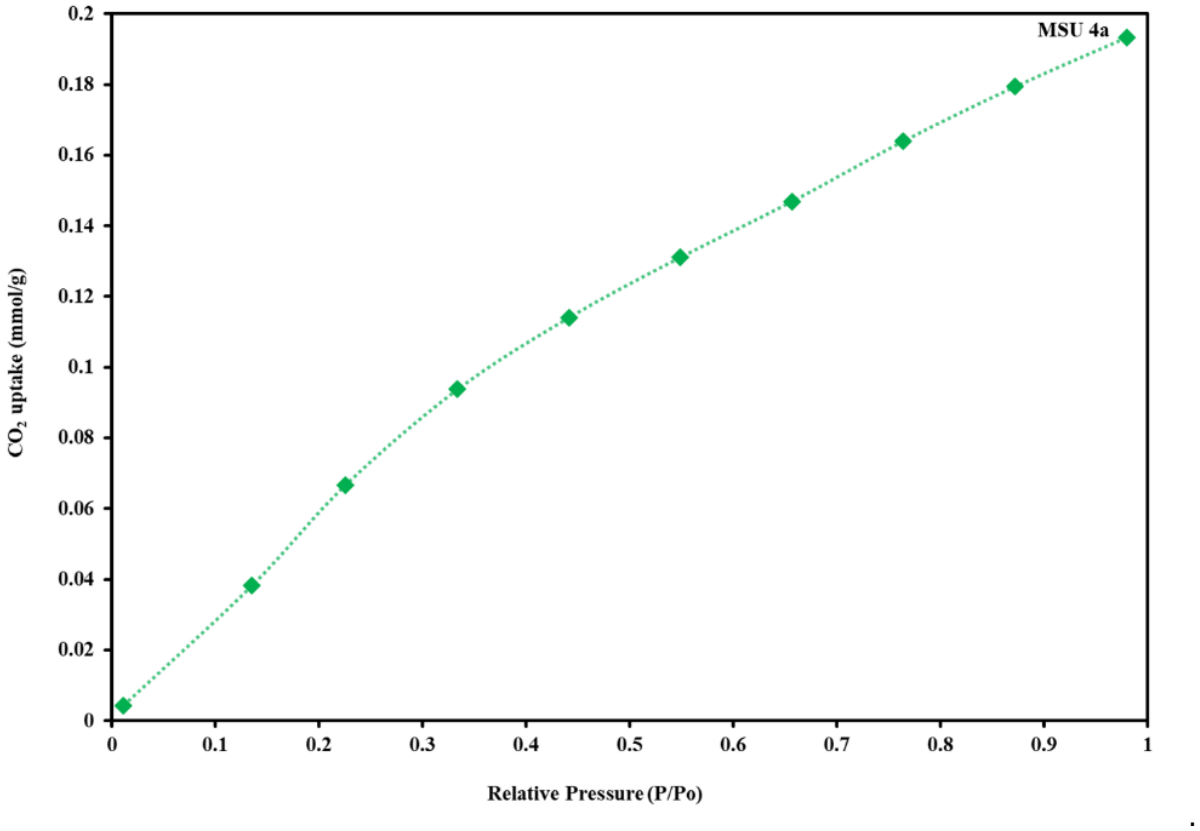

Figure 4.12: CO_2 adsorption-desorption isotherms for **MSU-4a** at 293 K.

4.12 Electrochemical characterisation

Figure 4.13a shows voltammetric responses of the bare and modified GCE (**MSU-4**) in a 5 mM $[Fe(CN)_6]^{3-/4-}$ solution containing 0.1 M KCl at 100 mVs^{-1}. It can be seen that the peak current (I_p) of $[Fe(CN)_6]^{3-/4-}$ increased and the peak-to-peak separation (ΔEp) decreased in the order of bare electrode and **MSU-4** as it is shown in Table 4.3.

To estimate the active area of MSU-4/GCE electrode, a solution of 5mM $[Fe(CN)_6]^{3-/4-}$ with 0.1 M KCl was used.

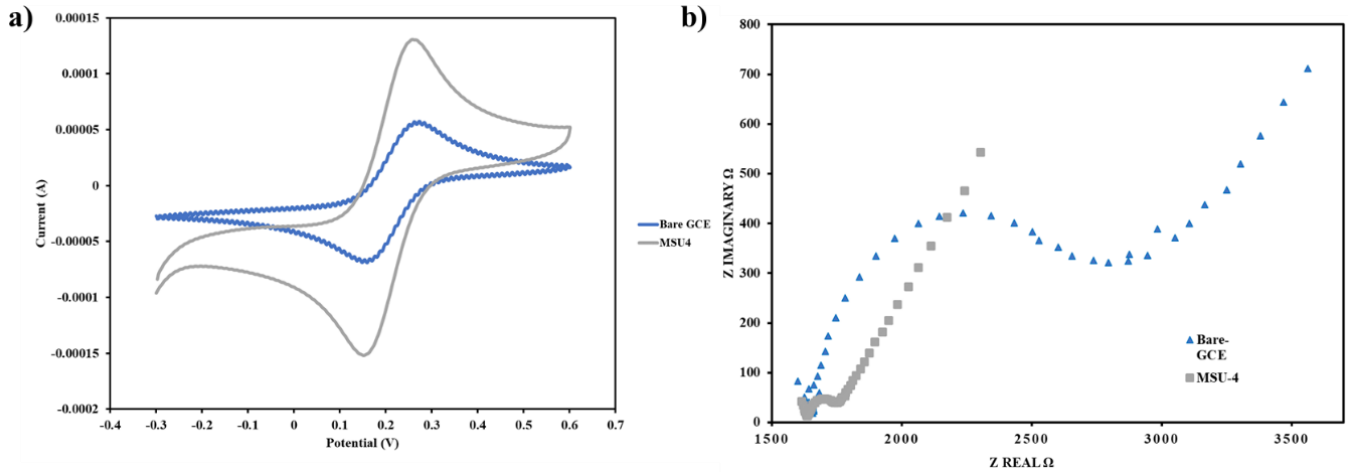

Figure 4.13: a) CVs of 5 mM $[Fe(CN)_6]^{3-/4-}$ at the bare GCE and **MSU-4** modified GCE electrode Scan rate 100 mVs^{-1} b) EIS of **bare GCE** and **MSU-4** modified electrode in 5mM $[Fe(CN)_6]^{3-/4-}$ solution containing 0.1M KCl.

Table 4.3 Δ Ep and Ipa values of all working electrodes.

Electrode	Δ Ep values	Ipa
GCE	0.12	53 µA
MSU-4	0.084	113 µA

Figure 4.13b shows the Nyquist plots of bare GCE and **MSU-4/GCE** in 5 mM $[Fe(CN)_6]^{3-/4-}$ containing 0.1 M KCl, respectively. The **MSU-4/GCE** showed a lower interfacial electron transfer resistance (113±5Ω) than that of bare GCE (115±5Ω). This suggests that the electron transfer is faster at MSU-4/GCE than that of bare GCE, which facilitates the arrival of the electrochemical probe to the surface of the electrode.

4.13 Surface area determination

The surface area of GCE and MSU-4/GCE were determined using the $[Fe(CN)_6]^{3-/4-}$ redox system and applying Randles-Sevcik Equation (4.1).

$$I_p = (2.69 \times 10^5) n^{3/2} A D^{1/2} V^{1/2} C \qquad \textbf{Equation 4.1}$$

where D is the diffusion coefficient (7.6 × 10 -6 cm^2s^{-1}) and C the bulk concentration of the redox probe (5mM $[K_3Fe(CN)_6]$ in 0.1 M KCl), n is the number of electron transferred (n = 1) and A_{eff} is the effective surface area. The surface area of the modified electrode was found to be 0.58 cm^2, which was twice larger than the bare glassy carbon electrode area 0.0719 cm^2.

4.14 Summary

lanthanum based MOF **(MSU-4)**, with molecular formulae $[Ce(H_2O)_2(bpdc)_{3/2}(DMF)\cdot 7(DMF)]$ was synthesised using 2,2'-bipyridine-5,5'-dicarboxylic acid and $Ce(NO_3)_3\cdot 6H_2O$ as starting materials. **MSU-4** crystallises in the triclinic crystal system, space group *P-1.* The overall structure is a three-dimensional (3D) structure. The activated phase of **MSU-4**, **MSU-4a**, was functionalised by cyclometallation of the MOF backbone using the metal precursor $[RuCl_2(p\text{-cymene})]_2$ to give **Ru(II)@MSU-4a.** PXRD analysis reveals a phase change induced by the inclusion of the [Ru(II)Cl(p-cymene)] in **MSU-4a**. The stability experiments show that the carboxylate moiety's binding mode is preserved in various chemical conditions. The ability to capture CO_2 was assessed using the activated phases of **MSU-4**. At 293 K, MSU-4 demonstrated noticeable carbon dioxide adsorption-desorption isotherms.

Electrochemical methods, i.e., cyclic voltammetry and electrochemical impedance spectroscopy were used to study the conductance of modified electrode, it showed very good electron transfer efficiency

4.15 References

1. Suresh, S. Jaisankar, V. Vinitha, G. & Kumar, R. M. Synthesis, structural, growth, optical, electrical, thermal and third order nonlinear optical properties of a organic single crystal: p -Toluidinium malonate. *J. Mol. Struct.***1202**, (2020).
2. Krause, L., Herbst-Irmer, R., Sheldrick, G. M. & Stalke, D. Comparison of silver and molybdenum microfocus X-ray sources for single-crystal structure determination. *J. Appl. Crystallogr.***48**, 3–10 (2015).
3. Sabouni, R., Kazemian, H. & Rohani, S. Carbon dioxide capturing technologies: A review focusing on metal organic framework materials (MOFs). *Environ. Sci. Pollut. Res.***21**, 5427–5449 (2014).
4. McArdle, P. SORTX - a program for on-screen stick-model editing and autosorting of SHELX files for use on a PC . *J. Appl. Crystallogr.***28**, 65–65 (1995).
5. Spek, A. L. Platon squeeze: A tool for the calculation of the disordered solvent contribution to the calculated structure factors. *Acta Crystallogr. Sect. C Struct. Chem.***71**, 9–18 (2015).
6. Barbour, L. J. X-seed - A software tool for supramolecular crystallography. *J. Supramol. Chem.***1**, 189–191 (2001).
7. C. F. Macrae, I. Sovago, S. J. Cottrell, P. T. A. Galek, P. McCabe, E. P. & M. Platings, G. P. Shields, J. S. Stevens, M. T. and P. A. W. The Genesis of the C. P. A. Movement. *J. Appl. Cryst.* **19**, 226–235 (2020)

Chapter 5: Conclusion

5.1 Summary

Metal Organic Frameworks (MOFs) are a family of crystalline porous materials, constructed through coordination between metal nodes and organic linkers.[1] MOFs consist of both inorganic and organic units. The organic units consist of carboxylates, or anions, such as phosphonate, sulfonate, and heterocyclic compounds. The inorganic units are the metal ions or clusters termed as secondary building block units (SBUs). Since MOFs are porous materials, they have received enduring interest in chemical science because of their suitability for many applications.

MOFs were selected as the main class of porous materials as they exhibit very high gas adsorption capacity for CO_2, H_2 and CH_4[2]. The large porosity allow their applications in separation of gases molecules and storage,[3] catalysis,[4] molecular sensing,[5] magnetism,[6] adsorption,[7] micro-electronics,[8] optics,[9] sensing application,[10] bioreactors,[11] drug delivery systems[12] and others. These porous solids are broadly classified into two major categories amorphous and crystalline.

The work presented in this thesis focused on the preparation and characterisation of MOFs using bipyridyl dicarboxylate linker, 2,2'-bipyridine-5,5'-dicarboxylate. After activation, the efficacy of the MOFs as storage devices of carbon dioxide and electrochemical properties were evaluated.

The MOFs were characterised using Fourier Transform Infrared Spectroscopy, Thermogravimetric analysis, Scanning Electron Microscopy-Energy Dispersive and Potentiostat Galvanostat Structural elucidation were performed by single-crystal X-ray diffraction and powder X-ray diffraction studies were used to check the phase purity

and phase transition of the prepared materials. Potentiostat Galvanostat was used to study electrochemical properties of the MOFs.

5.1.1 MSU-3

A 3D metal-organic frameworks, **MSU-3**, with the molecular formula $[Ce(bpdc)_4(H_2O)_2]$ was obtained under solvothermal conditions using 2,2'-bipyridine-5,5'-dicarboxylic acid and $Ce(NO_3)_3{\cdot}6H_2O$ at 120 ºC. **MSU-3** crystallises in the monoclinic crystal system, space group $P2_1/c$. The structure of **MSU-3** is made up of $Ce_2C_4O_4$ secondary building unit (SBU) rods which grow along a-b plane. Analysis of the channels of **MSU-3** using PLATON shows that they occupy 16.4 % of the unit cell volume.

Thermogravimetric analysis of **MSU-3** revealed a 4.7% weight loss which corresponds to the loss of two water molecules per formula unit modelled in the structure of **MSU-3** (calculated 3.8%). The framework decomposes around 325 °C. **MSU-3** was activated by soaking the as-made crystals in methanol for 24 hours, followed by heating under vacuum for 24 hours at 160 °C to give the activated phase, **MSU-3a**. PXRD analysis revealed that the structural integrity of the framework is maintained upon the evacuation of the guest molecules.

To test the chemical stability, the activated MOF, **MSU-3a** was soaked in different organic solvents for 24 hours. The PXRD patterns of recovered samples indicate that **MSU-3a** retains the original framework suggesting high chemical stability except in water where there is transformation. CO_2 sorption at 293 K reveals surface areas of 0.57 cm^2. The adsorption measurements at various temperatures revealed a Type-I isotherm, which is typical of microporous materials. **MSU-3a** gave volumetric uptake of 3.86 cm^3 (STP) g^{-1} (0.164799 $mmolg^{-1}$) whilst **Ru(II)@MSU-3a** gave a volumetric

uptake of 2.22 cm^3 (STP) g^{-1} (0.09487 $mmolg^{-1}$). **MSU-3a** was tested for electroactivity in 5 mM $[Fe(CN)_6]^{3-/4-}$. Also resistivity was tested using electrical impedance spectroscopy, It was found out that it had a lower interfacial electron transfer resistance (113±5Ω).

5.1.2 MSU-4

MSU-4 crystallises in a triclinic crystal system and space group P-1. The structure of **MSU-4** comprises $Ce_2C_2O_4$ rod SBU which grows along the a-axis. The channels in **MSU-4**, constitutes 51.6% of the unit cell volume as estimated by PLATON. The thermal analysis of MSU-4 shows an initial weight loss of 61.5% which corresponds to the elimination of 8 DMFs per unit modelled in the structure (calculated 61.1%) between 25 and 80 ^oC. The structure decomposes at 380 ^oC. PXRD analysis revealed that the structural integrity of the framework is maintained upon activation.

Chemical stability studies of **MSU-4** were carried out by soaking the activated phase in different organic solvents for 24 hours. The results of the PXRD patterns revealed that **MSU-4a** retains the original framework except in water where there is some transformation. CO_2 sorption at 293 K reveals surface areas of 0.58 cm^2. The adsorption measurements at various temperatures revealed a Type-I isotherm, which is typical of microporous materials. **MSU-4a** gave a volumetric uptake of 4.44 cm^3 (STP) g^{-1} (0.19 $mmolg^{-1}$) at 293 K. **MSU-4a** was tested for electroactivity in 5 mM $[Fe(CN)_6]^{3-/4-}$. Also resistivity was tested using electrical impedance spectroscopy, It was found out that it had a lower interfacial electron transfer resistance (113 ± 5Ω).

5.2 References

1. Wang, J. Yilmaz, E. Zhang, X. Li, H. Zhang, R. Guo, X. Sun, H. Hydration Energetics of a Diamine-Appended Metal-Organic Framework Carbon Capture Sorbent. *J. Phys. Chem. C***124**, 398–403 (2020).

2. Liang, J. Huang, Y. & Cao, R. Metal – organic frameworks and porous organic polymers for sustainable fixation of carbon dioxide into cyclic carbonates. *Coord. Chem. Rev.***3**, 332-345 (2017).

3. Liang, L. Liu, C. Jiang, F. Chen, Q. Zhang, L. Xue, H. Jiang,H. Quan, J. Yuan,D. Carbon dioxide capture and conversion by an acid-base resistant metal-organic framework. *Nat. Commun.***8**, 879- 940 (2017).

4. Kortlever, R., Shen, J., Schouten, K. J. P., Calle-Vallejo, F. & Koper, M. T. M. Catalysts and Reaction Pathways for the Electrochemical Reduction of Carbon Dioxide. *J. Phys. Chem. Lett.***6**, 4073–4082 (2015).

5. Gennaro, A. Isse, A. Severin, M. Vianello, E. Bhugun, I. Saveant, J. Mechanism of the electrochemical reduction of carbon dioxide at inert electrodes in media of low proton availability. *J. Chem. Soc. - Faraday Trans.***92**, 3963–3968 (1996).

6. Li, J., Wang, Y., Chen, Y. & Kung, C. applied sciences Metal – Organic Frameworks Toward Electrocatalytic Applications. *J. Appl. Crystallogr.***11**, 361–382 (2019).

7. Arana, C., Yan, S., Keshavarz, K. M., Potts, K. T. & Abruña, H. D. Electrocatalytic Reduction of Carbon Dioxide with Iron, Cobalt, and Nickel Complexes of Terdentate Ligands. *Inorg. Chem.***31**, 3680–3682 (1992).

8. Al-Omari, A. A., Yamani, Z. H. & Nguyen, H. L. Electrocatalytic CO2 reduction:

From homogeneous catalysts to heterogeneous-based reticular chemistry. *Molecules* **23**, 1–12 (2018).

9. Krause, L., Herbst-Irmer, R., Sheldrick, G. M. & Stalke, D. Comparison of silver and molybdenum microfocus X-ray sources for single-crystal structure determination. *J. Appl. Crystallogr.***48**, 3–10 (2015).

10. Fiedorow, R. M. J., Chahar, B. S. & Wanke, S. E. The sintering of supported metal catalysts. II. Comparison of sintering rates of supported Pt, Ir, and Rh catalysts in hydrogen and oxygen. *J. Catal.***51**, 193–202 (1978).

11. Meilikhov, M. Yusenko, K. Esken, D. Turner, S. Tendeloo, G. Fischer,R. Metals @ MOFs – Loading MOFs with Metal Nanoparticles for Hybrid Functions. *J. Appl. Crystallogr.* **12***,* 3701–3714 (2010)

12. Liu, B. Vellingiri, K. Jo, S. Kumar, P. Sik OK, Y. Kim, K. Recent advances in controlled modification of the size and morphology of metal-organic frameworks. *Nano Res.***11**, 4441–4467 (2018).